IEEE Access
Multidisciplinary | Rapid Review | Open Access Journal

Received 21 March 2023, accepted 18 April 2023, date of publication 24 April 2023, date of current version 3 May 2023.

Digital Object Identifier 10.1109/ACCESS.2023.3269584

RESEARCH ARTICLE

Unified Quality-Aware Compression and Pulse-Respiration Rates Estimation Framework for Reducing Energy Consumption and False Alarms of Wearable PPG Monitoring Devices

GANGIREDDY NARENDRA KUMAR REDDY[1], (Member, IEEE), M. SABARIMALAI MANIKANDAN[1,2], (Senior Member, IEEE), N. V. L. NARASIMHA MURTY[3], (Member, IEEE), AND LINGA REDDY CENKERAMADDI[4], (Senior Member, IEEE)

[1]Indian Institute of Technology Bhubaneswar, Bhubaneswar, Odisha 752050, India
[2]Indian Institute of Technology Palakkad, Palakkad, Kerala 678623, India
[3]Indian Institute of Technology Tirupati, Tirupati, Andhra Pradesh 517619, India
[4]Department of ICT, University of Agder, NO-4879 Grimstad, Norway

Corresponding author: Linga Reddy Cenkeramaddi (linga.cenkeramaddi@uia.no)

This work was supported in part by the International Partnerships for Excellent Education, Research and Innovation (INTPART) Program from the Research Council of Norway through the Indo-Norwegian Collaboration in Autonomous Cyber-Physical Systems (INCAPS) Project from the Research Council of Norway under Grant 287918. The work of Gangireddy Narendra Kumar Reddy was supported in part by the Council of Scientific and Industrial Research (CSIR) Fellow under Grant 09/1059/ (0010)2015-EMR-1; in part by the Extra Mural Research Division, New Delhi, and the Indian Institute of Technology Bhubaneswar, Odisha, India, through the thesis titled "Unified Quality-Aware Data Compression and Pulse-and Respiration-Rate Extraction Frameworks for Resource-Constrained Wearable Health Monitoring Devices."

ABSTRACT Due to the high demands of tiny, compact, lightweight, and low-cost photoplethysmogram (PPG) monitoring devices, these devices are resource-constrained including limited battery power. Consequently, it highly demands frequent charge or battery replacement in the case of continuous PPG sensing and transmission. Further, PPG signals are often severely corrupted under ambulatory and exercise recording conditions, leading to frequent false alarms. In this paper, we propose a unified quality-aware compression and pulse-respiration rates estimation framework for reducing energy consumption and false alarms of wearable and edge PPG monitoring devices by exploring predictive coding techniques for jointly performing signal quality assessment (SQA), data compression and pulse rate (PR) and respiration rate (RR) estimation without the use of different domains of signal processing techniques that can be achieved by using the features extracted from the smoothed prediction error signal. By using the five standard PPG databases, the performance of the proposed unified framework is evaluated in terms of compression ratio (CR), mean absolute error (MAE), false alarm reduction rate (FARR), processing time (PT) and energy saving (ES). The compression, PR, RR estimation, and SQA results are compared with the existing methods and results of uncompressed PPG signals with sampling rates of 125 Hz and 25 Hz. The proposed unified quality-aware framework achieves an average CR of 4%, SQA (Se of 92.00%, FARR of 84.87%), PR (MAE: 0.46 $\pm$1.20) and RR (MAE: 1.75 (0.65-4.45), PT (sec) of 15.34 $\pm$0.01) and ES of 70.28% which outperforms the results of uncompressed PPG signal with a sampling rate of 125 Hz. Arduino Due computing platform-based implementation demonstrates the real-time feasibility of the proposed unified quality-aware PR-RR estimation and data compression and transmission framework on the limited computational resources. Thus, it has great potential in improving energy-efficiency and trustworthiness of wearable and edge PPG monitoring devices.

INDEX TERMS Photoplethysmogram (PPG), PPG data compression, pulse rate measurement, respiration rate measurement, wearable devices, Internet of Medical Things, energy-constrained PPG devices.

The associate editor coordinating the review of this manuscript and approving it for publication was Lorenzo Mucchi.

I. INTRODUCTION

Rapid technological advancements and disruptive innovations across various technologies, including ultra-miniaturized biosensors, low-power flexible and stretchable electronics, ultra-low power high-resolution data acquisition, low-power high-speed processors, and ultra-low power higher data-rate wireless radio have resulted in the development of ultra-lightweight and compact wireless wearables that can be easily worn on the body or conveniently attached to a person's body. These wireless wearables are also called smart sensing devices or smart electronic devices which are more convenient to wear, sense, analyze and interpret in real-time, store and seamlessly transmit the data to a next-level computing platform or other smart devices in wireless body area networks (WBANs) or internet of medical things (IoMT) based fitness and health monitoring applications [1], [2], [3], [4]. The rapid pace of advancements in miniaturization and integration enables the integration of heterogeneous sensors into wearables that are nearly invisible to an individual. Thus, modern wireless wearable devices have received tremendous attention in today's global wearable fitness and healthcare monitoring device markets that can find huge potential in the real-time monitoring of vital signs or critical biomarkers, point-of-care diagnosis, virtual clinical trials, and drug delivery, psycho-physiological stress monitoring, determining individual's health status, and ubiquitous, continuous, and personal fitness monitoring, including the physical and posture patterns, and daily energy expenditure [5], [6], [7], [8], [9], [10].

A. WHY PPG SENSING IS POPULAR?

The Internet of Things (IoT) and Smartphone technologies based health monitoring devices play a major role in transforming and revolutionizing personal healthcare systems by continuous monitoring of the health status of an individual and timely notifying caregivers [10], [11], [12], [13]. Among sensing of biosignals such as electrocardiogram (ECG), phonocardiogram (PCG), photoplethysmogram (PPG) in health monitoring applications, PPG sensing has become most popular because (*i*) it enables measurement of different kinds of vital signs such as pulse rate (PR), respiration rate (RR), blood pressure (BP), blood glucose level (BGL), blood oxygen saturation (SpO2), (*ii*) it can be used to understand the emotional states of an individual, and (*iii*) it can be easily sensed with a simple and low-cost hardware and also it is more comfortable in continuous monitoring under different kinds of daily activities as compared to other biosignal sensing.

B. KEY LIMITATIONS OF EXISTING PPG PROCESSING SYSTEMS

Although there are huge technological advancements in wearable or portable health monitoring devices, there are many challenges that need to be addressed: (*i*) Frequent false alarms due to unavoidable motion artifacts, signal saturation, and other noises in continuous health monitoring scenarios [14], [15], [16], [17], [18], [19]; (*ii*) limited battery power leads to a key challenge to the continuous sensing, processing, and transmission of data wirelessly to the remote server [17], [18], [19], [20]; (*iii*) frequent sensor's disconnection or movements under ambulatory or exercise conditions [14]; and (*iv*) malfunctioning of sensor and battery leads to the signal saturation or clipping [21]. By considering the significance of the quality of the PPG signal, there is a need for exploring lightweight signal quality assessment (SQA) or signal quality indicator (SQI) for discarding the noisy PPG signals since the distorted PPG may produce noisy pulse measurements which can lead to inaccurate or unreliable diagnosis [3], [21].

From the past PPG data compression studies as reported in the literature, it can be observed that achieving a high compression ratio is the main objective of existing methods at the cost of computational resources including the battery power, high-speed processor, and memory space [3], [22]. Furthermore, real-time implementation of PPG data compression was not addressed in past studies by considering the constraints of wearable PPG sensing devices. Moreover, energy consumption analysis was not studied which is most important not only for computing the percentage of energy saving but also for knowing the energy consumption of the compression method. Further, most compression methods can enable higher compression of PPG signals but are not suitable for extracting the vital parameter(s) directly in the compressed domain or not an integral part of compressed algorithms [3], [22]. In such scenarios, additional signal processing techniques were used to first reconstruct the original PPG signal for estimating the PR and/or RR parameter(s) in real-time or on-device vital sign estimation application that demands more computational power and resources which are constraints of affordable wearable multi-parameter health monitoring devices. Thus, for resource-constrained devices, exploring lightweight data compression is essential that can enable the estimation of vital signs at the sensing node or on-device in order to provide intelligence (or notify) the user and also reduce the latency or processing time for timely triggering other drug delivery or sensing devices.

C. RESOURCE-CONSTRAINED WEARABLES AND ITS ENERGY EFFICIENCY REQUIREMENT

Wearable or portable monitoring devices are constrained with limited power due to the device's miniaturization with the use of a tiny battery. Thus, such a device demands frequent charging or replacement of batteries, which can be inconvenient or uncomfortable for the end users. Energy efficiency (or low energy consumption) is a critical requirement for battery-operated wireless wearable devices. For most health and wellness monitoring application scenarios, wearable PPG monitoring devices are generally designed to perform the following tasks: sensing PPG signal(s), processing the sensed data (or on-device or on-board parameter extraction), and

transmitting the original or processed data to the remote server [21]. Each functional task can significantly contribute to the energy consumption at the device and thereby impact the battery life-time in continuous PPG sensing, processing, and transmission [21]. In addition to these tasks, storing the large amount of data generated in continuous monitoring consumes a considerable amount of energy.

D. SIGNIFICANCE OF JOINT PPG SIGNAL PROCESSING TASKS

A few research works were presented for reducing energy consumption or prolonging battery life. A few studies considered the data compression and/or wireless transmission control for reducing the energy consumption of wireless data transmission but the real-time implementation of such approaches is not addressed by considering computational resource constraints of wearable devices [17], [18], [19], [20]. By considering resource-constraints, there is a need to perform a joint signal quality assessment, compression, and parameter extraction without using multiple domain signal processing techniques for each of the processing tasks by exploring lightweight signal processing technique(s). Further, we noticed that existing PR methods based on the Fourier magnitude, autocorrelation, and multiplication factor techniques had poor estimation accuracy under both abnormal PPG signals with time-varying pulse-to-pulse intervals and waveform shape morphologies, and noisy PPG signals [23].

In past studies, to the best of our knowledge, there is no attempt for the design of a resource-efficient unified PPG signal processing framework that can enable integrated or combined signal quality assessment, data compression, and PR-RR parameter extraction tasks without the use of such signal processing techniques. The rest of this paper is organized as follows. Section II presents the major contributions of this paper. Section III presents the proposed quality-aware predictive coding-based joint signal quality assessment, compression, and PR-RR parameter extraction framework. Section IV presents evaluation results for each of the PPG signal processing tasks. Section V presents the real-time implementation of the proposed unified predictive coding-based quality-aware data compression and PR-RR estimation framework. Finally, conclusions are presented in Section VI.

II. MAJOR CONTRIBUTIONS OF THIS PAPER

In this paper, a unified predictive coding-based quality-aware data compression and pulse- and respiration-rate estimation framework is proposed for energy-constrained wearable and edge PPG monitoring devices, as shown in Fig. 1. The main aim of this paper is to minimize the total energy consumption by exploring predictive coding techniques for performing joint signal quality, data compression, and parameter extraction without the use of different domains of signal processing techniques and also performing the signal quality assessment by using the features extracted from the smoothed predictive error signal. The proposed quality-aware unified framework can enable quality-aware data compression and transmission and also quality-aware parameter extraction which can significantly reduce energy consumption and false alarm rate by discarding the severely corrupted PPG signals, which are unavoidable in wearable PPG monitoring application scenarios. Based on the predictive coding technique, the key contributions of this paper are summarized below:

- Simple PPG compression method is presented using the concept of predictive coding wherein the prediction error signal is encoded with less number of bits (2 to 4 bit), as compared to the original sample resolution.
- Automatic PPG signal quality assessment (PPG-SQA) method is presented based on the predictive coefficient and time-domain features extracted from the quantized prediction error signal and performance is evaluated using a wide variety of motion artifacts and noises.
- An automatic PR estimation method is presented based on the number of systolic peaks (NSPs) and average pulse-to-pulse intervals (PPIs) extracted from the smoothed prediction error signal. The measurement results are compared with the fast Fourier transform (FFT) and autocorrelation function (ACF) based PR estimation methods and also other existing methods.
- An automatic RR estimation methods are presented by measuring respiratory-induced variations such as respiratory-induced amplitude variation (RIAV), respiratory-induced intensity variation (RIIV), respiratory-induced frequency variation (RIFV) from the original PPG signal-based candidate locations of onset and systolic peaks, which are determined by processing the smoothed prediction error signal. The best RR estimation method is highlighted and its performance is compared with other existing methods.
- Finally, unified quality-aware data compression and PR-RR estimation framework for reducing energy consumption and false alarms by discarding severely corrupted PPG signals from further processing tasks and this unified framework is implemented on the Arduino computing platform for demonstrating real-time feasibility and energy saving.

A. DESCRIPTION OF TEST DATABASES

For performance evaluation, a wide variety of PPG signals is considered for understanding different kinds of waveform distortions and the robustness of the proposed methods. The PPG signals are taken from the standard databases, including the Multiparameter intelligent monitoring in intensive care II (MIMIC-II), the MIT-BIH Polysomnographic (MITBIH-SLP), the CapnoBase (336 segments, http://www.capnobase.org/; from 59 children (median age: 8.7, range: 0.8 - 16.5 years) and 35 adults (median age: 52.4, range: 26.2 - 75.6 years)), the Complex Systems Laboratory (CSL, 118 segments) [53], and other recording databases (621 segments), and Beth Israel Deaconess Medical Centre (BIDMC, 424 segments; (median age: 64.81, range: 19-90+,

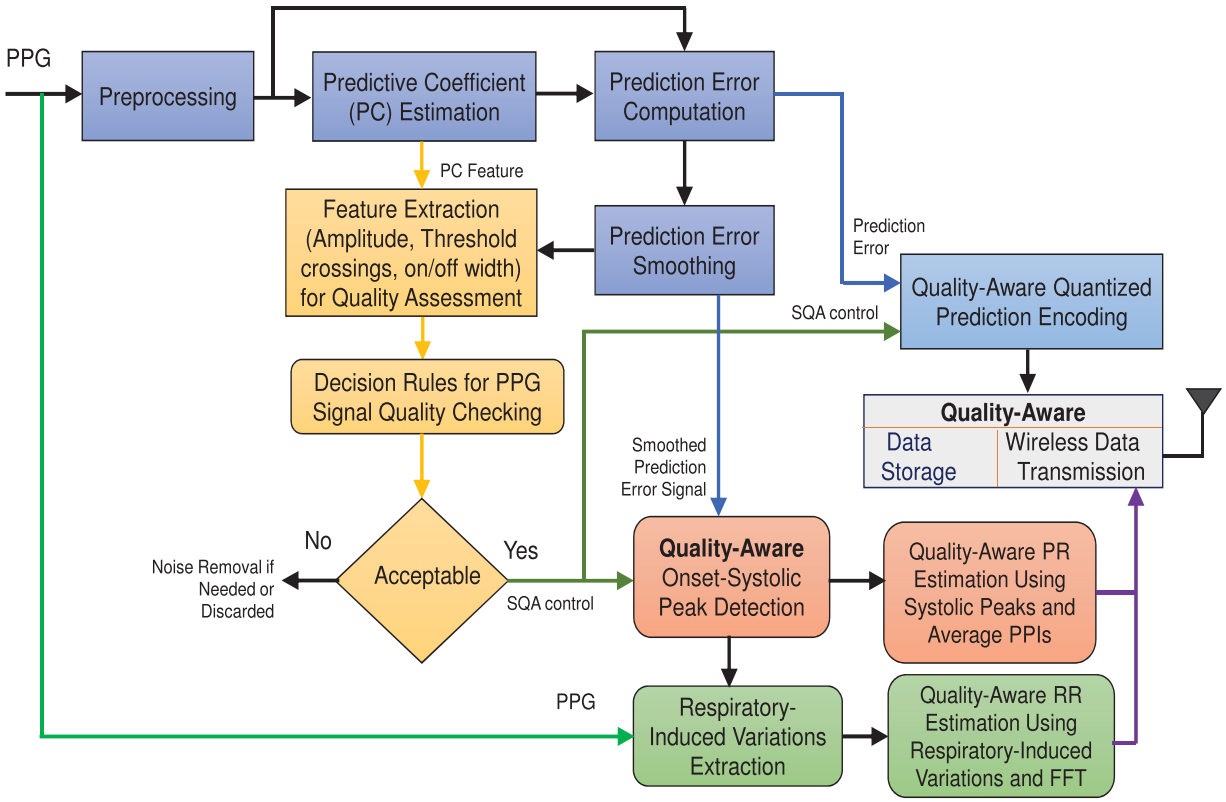

FIGURE 1. Block diagram of a unified predictive coding based quality-aware data compression and PR-RR estimation framework.

32 females and 21 males)). The MIT-BIH SLP database (subjects with age ranging from 32 to 56) includes the recordings of multiple physiologic signals during sleep [54]. The PPG records "slp01a" and "slp01b" are segments of one subject's polysomnogram, separated by a gap of about one hour. The PPG records "slp02a" and "slp02b" are segments of another subject's polysomnogram, separated by a ten-minute gap. The signals were digitized at a sampling frequency of 250 Hz and 12 bits/sample. From the MIT-BIH Polysomnographic database (MIT-BIH SLP), 1071 segments were considered for the performance evaluation. From the MIMIC database (aged 16 years or above) with 03700001m -03700020m, 186 segments were considered. From the MIMIC-III(p026377-2111-11-17-16-46m, p075796-2198-07-25-23-40m, AF events), we considered the 138 segments. From the MIMIC-III (p007614-2177-01-08-13-21m, p030542-2135-10-17-10-33m, p065656-2121-08-07-04-35m), we considered the 130 PVC/PAC segments. From the MIMIC-III (p004829-2103-08-30-21-52m, p013072-2194-01-22-16-13m, p050384-2195-01-30-02-21m, p055204-2132-06-30-09-34m p058932-2120-10-13-23-15m), we considered the NSR of 150 segments) that available at https://archive.physionet.org/cgi-bin/atm/ATM. The CSL database contains six 60 min manually annotated recordings from six patients that were acquired by a data acquisition system in the complex systems laboratory (CSL) [53]. The recordings were sampled at 125 Hz, band-pass filtered and auto-scaled. It contains manual beat annotations from two independent experts and automatic annotations from the CSL Reference algorithm. The wrist database was collected from 8 participants (3 male, 5 female), age group between 22-32 years (mean age 26.5 years) during different physiological exercises such as bike riding and walking and running on a treadmill with variable speeds and time-intervals. The signals were digitized with a sampling rate of 256 Hz. The IEEE signal processing cup 2015 database consists of PPG signals recorded from the wrist using a pulse oximeter with green LED (609nm) and three-axis accelerometer signals. These databases were collected from the subjects 12 males with yellow skin in the age group 18-35 years. All the signals were digitized with a sampling rate of 125 Hz. The performance of signal quality assessment is tested by Noise-free PPG (NFPPG) of 109503 segments, Motion Artefact PPG considered from wrist and cup database of 99036 segments and Motion Artefact PPG considered from acceleration signals of 101568 segments, Pulse Free PPG (PF PPG) signals generated from random noise of 101568 segments. The segment duration is 5 seconds

and the sampling frequency is 125 Hz for the SQA test. Motion artefact (MA) corrupted PPG signals are created by acceleration signals taken from the cup database with different levels (0.5, 0.7, 0.9) by using the following equation. $y[n]$ is the MA PPG signal generated from the acceleration signal.

$$y[n] = x[n] + w * acc[n], \tag{1}$$

where $x[n]$ is the normalized noise-free PPG signal (Total 3174 NF PPG 60 seconds segments are used) after removing the mean from the original noise-free PPG signal and $acc[n]$ is the normalized acceleration signal after removing mean from the signal. Here, w denotes the amplitude level that is fixed to 0.5, 0.7 and 0.9 in this study. For each amplitude level, 33856 segments are generated with an acceleration signal for the performance study. Pulse free PPG signals are created by random noise with different amplitude levels (0.5, 0.7, 0.9) by using the following equation.

$$z[n] = x[n] + w * r[n], \tag{2}$$

where $x[n]$ is the normalized noise-free PPG signal (A total of 3174 NF PPG segments are used) after removing the mean from the original noise-free PPG signal and $r[n]$ is the normalized random noise after removing the mean from the random signal. Here, w denotes the amplitude level that is fixed to 0.5, 0.7 and 0.9. For each amplitude level, 33856 segments are generated with random noises. $z[n]$ is the pule free PPG signal.

In the following sections, we present the time-domain feature-based PPG signal quality assessment method, predictive coding-based PPG compression method, prediction error-based onset-peak detection method and pulse- and respiration rate extraction method.

III. PROPOSED QUALITY-AWARE PPG COMPRESSION AND PARAMETER EXTRACTION METHODS

The main objective of this paper is to explore a lightweight signal processing technique that can enable simultaneous combined PPG processing tasks without the use of many additional signal processing technique(s) that can be performed using one or two signal processing technique(s) in the same processing domain and/or using features extracted from the same candidate signal obtained in the same signal processing domain (like, time-domain, frequency-domain, transform-domain, decomposition and prediction model domain). This paper presents the predictive coding-based simultaneous pulse and respiration rates extraction and compression which have great potential in reducing the overall energy consumption of wearable devices.

A. PROPOSED TIME-DOMAIN FEATURE BASED PPG SIGNAL QUALITY ASSESSMENT METHODS

Various SQA methods were presented for checking quality or detecting the presence of movement artifacts and noises (MAN). But real-time evaluation of the method was performed in terms of computational time and energy consumption which is most important to demonstrate energy saving or energy efficiency [17]. Without these performance metrics in addition to the better accuracy, it is difficult to recommend the best SQA methods for resource-constrained monitoring devices. Furthermore, there is a unified framework that can address the discrimination of noise-free PPG signals from noisy signals; timely notifying the sensor's disconnection; and timely detecting the signal saturation.

In many SQA methods, sets of fiducial and non-fiducial features were extracted from the original and filtered sensor signals, and differenced sensor signals by processing with different signal processing techniques such as digital filters, short-term Fourier transform (STFT), wavelet transform (WT), empirical mode decomposition (EMD), ensemble EMD (EEMD) and variational mode decomposition (VMD), independent component analysis (ICA) and adaptive filters [2], [14], [21]. However, the computational complexity of the methods was not addressed with reference to resource-constrained on-device processing in past studies. The design criteria behind most of them correspond to achieving high accuracy but the computational complexity and energy consumption were neglected, which is our primary goal.

In this paper, a new discriminative feature is explored based upon the extensive analysis of four time-domain features such as the number of threshold crossings (NTC), maximum and minimum amplitudes, on-width and off-width durations and first-order predictor coefficient (α) for automatically checking the quality of recorded PPG signals. The proposed SQA method is based on the above-mentioned time-domain features and predictor coefficient extracted from the prediction error signal that can be easily integrated with predictive coding-based PPG data compression. Unlike existing methods, the proposed method does not require beat detection, template creation, an updating process, and dynamic time warping (DTW) [19], [21], [23], [24], [25], [26], [27], The proposed SQA method can detect corrupted PPG segments, signal saturation, and sensor's disconnection but existing SQA methods can perform only MAN corrupted PPG segments [21].

1) LINEAR PREDICTIVE COEFFICIENT

The PPG signal consists of a slowly varying pulsatile component with a significant intra-beat correlation between successive samples [28]. Further, PPG signals are quasi-periodic signals exhibiting inter-beat correlation due to the repeated nature of heart function that leads to having higher redundancy or correlation between consecutive samples of a PPG signal. Thus, the bit rate can be reduced by exploring the sample redundancy using the linear prediction technique. The linear predictive coding can enable PPG data compression by storing or sending the encoded sample difference since the difference between adjacent samples is smaller than

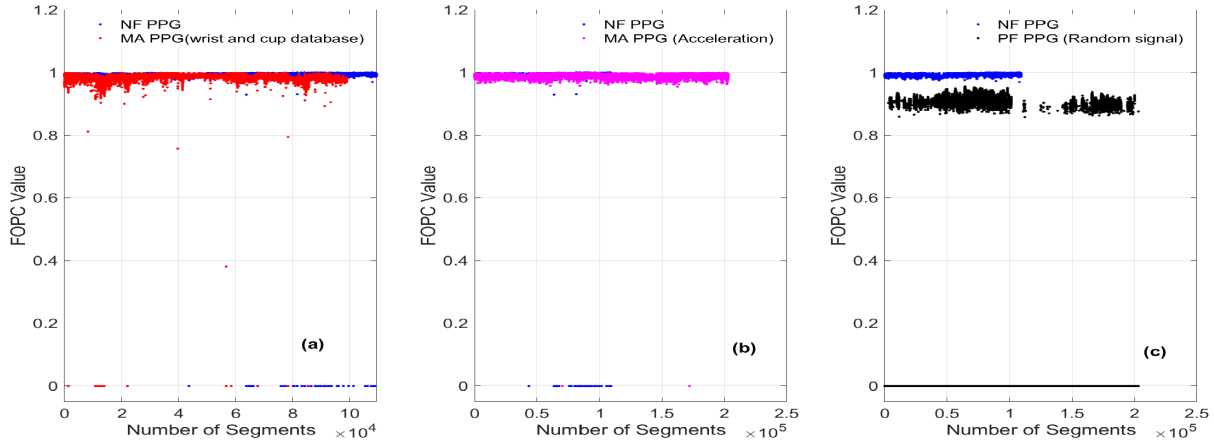

FIGURE 2. Estimated first order predictive coefficient (FOPC) from (*i*) noise-free PPG signals, (*ii*) movement artifact corrupted PPG signals taken from the wrist and cup databases, (*iii*) movement corrupted PPG signals created using the acceleration signals with different levels and (*iv*) noisy PPG signals created using additive white noises with different amplitude levels.

the original samples. In this section, an estimation of best predictor coefficients is briefly described. In linear prediction process [29], the predicted signal $\hat{x}[n]$ can be obtained as

$$\hat{x}[n] = \sum_{k=1}^{P} \alpha_k x[n-k] \tag{3}$$

where P denotes the predictive order and α_k denotes k^{th} predictive coefficients. The best predictor coefficients α_j are normally obtained by minimizing a mean-squared error criterion [29]. The prediction error between the predicted value and the actual value is computed as

$$e[n] = x[n] - \hat{x}[n] = x[n] - \sum_{k=1}^{P} \alpha_k x[n-k]. \tag{4}$$

The mean-squared prediction error is computed as

$$E\left[e^2[n]\right] = E\left[\left(x[n] - \sum_{k=1}^{p} \alpha_k x[n-k]\right)^2\right] \tag{5}$$

If we simplify the above expression, we can get

$$E\left[e^2[n]\right] = r_{xx}(0) - 2\mathbf{r}_{\mathbf{xx}}^{\mathbf{T}}\alpha + \alpha^{\mathbf{T}}\mathbf{R}_{\mathbf{xx}}\alpha, \tag{6}$$

where $\mathbf{R_{xx}} = E[xx^T]$ is the autocorrelation matrix of the input signal with a length of N, $\mathbf{r_{xx}}$ is the autocorrelation of the signal. From the above Equation (6), the gradient of the mean square prediction error with respect to the predictor coefficient vector α is given by

$$\frac{\partial}{\partial \alpha} E\left[e^2[n]\right] = -2\mathbf{r}_{\mathbf{xx}}^{\mathbf{T}}\alpha + 2\alpha^{\mathbf{T}}\mathbf{R}_{\mathbf{xx}}, \tag{7}$$

The least mean square error solution, obtained by setting Equation (7) to zero, is given by

$$\mathbf{R_{xx}} = \alpha \mathbf{r_{xx}}, \tag{8}$$

From Equation (8) the predictor coefficient vector is given by

$$\alpha = \mathbf{R}_{\mathbf{xx}}^{-\mathbf{1}}\mathbf{r}_{\mathbf{xx}}, \tag{9}$$

An efficient method for the solution of Equation (9) is the Levinson–Durbin recursive algorithm where $\mathbf{R_{xx}}$ is a Hermitian, positive-definite and Toeplitz matrix [29]. The zeroth estimation of error is given by

$$E^{(0)} = R(0). \tag{10}$$

The coefficients k_i are referred to as the reflection coefficients which can be computed as

$$k_i = \frac{[R(i) - \sum_{j=1}^{i-1} \alpha_j^{(i-1)} R(i-j)]}{E^{(i-1)}}, \quad 1 \le i \le P. \tag{11}$$

For i^{th} iteration, the predictor coefficient is computed as

$$\alpha_i^{(i)} = k_i. \tag{12}$$

$$\alpha_j^{(i)} = \alpha_j^{(i-1)} - k_i \alpha_{i-j}^{(i-1)} \quad 1 \le j \le i-1 \tag{13}$$

$$E^{(i)} = (1 - k_i^2) E^{(i-1)} \tag{14}$$

Equations (11) and (12) can be solved recursively for $i = 1, 2, \ldots P$. Then the final solution is

$$\alpha_j = \alpha_j^P \quad \text{for } 1 \le j \le P. \tag{15}$$

For prediction order, $P = 1$, the best predictor coefficient, $\alpha_1^{(1)}$ is computed as

$$E^{(0)} = R(0) \quad \text{and} \quad k_1 = \frac{R(1)}{E^{(0)}} \tag{16}$$

$$\alpha_1^{(1)} = k_1 = \frac{R(1)}{E^{(0)}} = \frac{R(1)}{R(0)} \tag{17}$$

where $\alpha_1^{(1)}$ denotes the first-order predictor coefficient (FOPC). Fig. 2 shows the estimated FOPC from (*i*) noise-free PPG signals, (*ii*) movement artifact corrupted PPG signals taken from the wrist and cup databases, (*iii*) movement

TABLE 1. Performance of signal quality assessment for different predictive coefficient values (α) in terms of sensitivity (Se)(%) and false alarm reduction rate (FARR) (%).

(NF: Noise-Free; PF: Pulse-Free and MA: Motion artifact]								
NF PPG vs MA PPG (wrist and cup database)			NF PPG vs MA PPG (Acceleration)			NF PPG vs PF PPG (Random Noise)		
(α)	Se	FARR	(α)	Se	FARR	(α)	Se	FARR
0.9893	90.16	52.97	0.9890	90.97	22.09	0.9554	99.87	100
0.9908	85.31	62.47	0.9908	85.33	36.78	0.9800	99.82	100
0.9918	80.52	69.85	0.9918	80.54	47.15	0.9890	90.92	100
0.9926	74.73	73.33	0.9934	66.61	66.50	0.9918	80.44	100

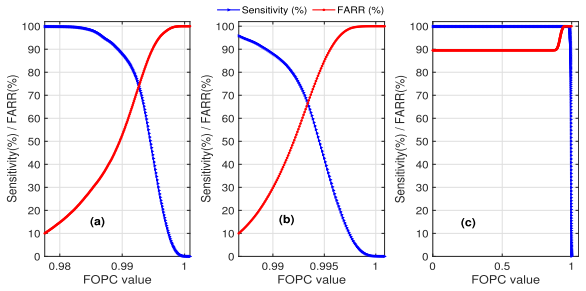

FIGURE 3. Performance of the first order predictive coefficient (FOPC) in terms of sensitivity (Se) and false alarm rate reduction (FARR) for (a) noise-free PPG and motion artifact PPG signals from wrist and cup database (b) noise-free PPG and motion artifact PPG signal generated from acceleration signals, and (c) noise-free PPG and random noise signals.

corrupted PPG signals created using the acceleration signals with different levels and (*iv*) noisy PPG signals created using additive white noises with different amplitude levels.

Evaluation results of the SQA method are summarized in Table 1 for noise-free (NF) PPG signals, noisy PPG signals taken from the wrist and cup databases, movement artifact (MA) corrupted PPG created using different kinds of acceleration signals with different magnitude levels, and noisy PPG signals corrupted with random noises with different kinds of magnitude levels. In order to select the optimal predictor coefficient threshold, the performance of the SQA method is evaluated in terms of sensitivity (Se) which measures the correct detection of noise-free PPG signals, and false alarm reduction rate (FARR) which measures the correct detection of noisy signals. Sensitivity (Se) and false alarm reduction rate (FARR) are computed as,

$$\text{Se} = \text{TP}/(\text{TP} + \text{FN}) \times 100\ \%, \tag{18}$$

$$\text{FARR} = \text{TN}/(\text{TN} + \text{FP}) \times 100\ \% \tag{19}$$

To compute Se and FARR, the following parameters are required: true positive (TP) when it is correctly detected the positive class (noise-free segments), false negative (FN) when it is not detected the negative class is, false positive (FP) when it is falsely detected the positive class and true negative (TN) when it is correctly detected the negative class (noisy segments). Fig. 3 illustrates the performance of the SQA for (a) noise-free PPG and motion artifact PPG signals from wrist and cup database (b) noise-free PPG and motion artifact ppg signal generated from acceleration signals and (c) noise-free PPG and random noise signals.

From preliminary evaluation results, it can be observed that sensitivity (Se) and false alarm reduction rates are better for the first-order predictive coefficient (FOPC) threshold of 0.9893. Higher sensitivity is most important so that noise-free PPG signals cannot be discarded from the parameter extraction and compression stages of the proposed unified framework. Results further show that the method had FARR of 100% and Se of 99.87% for the coefficient threshold of 0.9554 for the noisy PPG signals corrupted with random noises. It can be also observed that the quality assessment results vary with the characteristics of noises and artifacts. However, the determination of a single coefficient threshold is most essential irrespective of the type of noises and artifacts. In this study, all the noisy PPG signals are merged to find optimal thresholds. This study shows that the Se of 93.67% and FARR of 58.35% can be achieved for an optimal coefficient threshold of 0.9893. In the result section, the performance of the signal quality assessment is further evaluated by using the other time-domain features which are described in the following subsections.

2) NUMBER OF THRESHOLD CROSSINGS AND MAXIMUM AMPLITUDE FEATURES

During ambulatory recordings, pulse-free signals are encountered due to the sensor's disconnection from a measurement site. The pulse-free signals may include different kinds of low-frequency and high-frequency noises with different amplitudes within the dynamic range of a device's operating voltage. The PPG sensing module with noise cancellation method may produce very-low amplitude pulse-free signals. Then, sensor disconnection may be detected by comparing maximum and minimum amplitudes of sensor signals with predefined amplitude thresholds by choosing based on the lowest amplitude range of the noise-free PPG signals that can be measured in both normal and abnormal PPG recordings as discussed in the previous section. However, in practice, pulse-free signals may include motion artifacts and other noises such as ambient light-induced noise, thermal noise, and power-line interference (50/60 Hz) [30]. In such scenarios, short-term amplitude features can be used for discriminating the PPG patterns from the noise patterns. It can be observed that the maximum amplitude (systolic peak) is higher than the minimum amplitude (foot) in the zero-mean sensor signal. The maximum and minimum amplitude features can be used to discriminate some of the pulse-free noisy and corrupted PPG signals. For high-amplitude pulse-free signals, the number of zero-crossings (NZC) can be explored to discriminate fast varying noise components by comparing with the NZC value of noise-free PPG signals with fixed block length and maximum number of cycles with a minimum PPI of 200 ms (i.e., 300 beats per minute (bpm)). For example, The higher NZC value represents the case of noisy

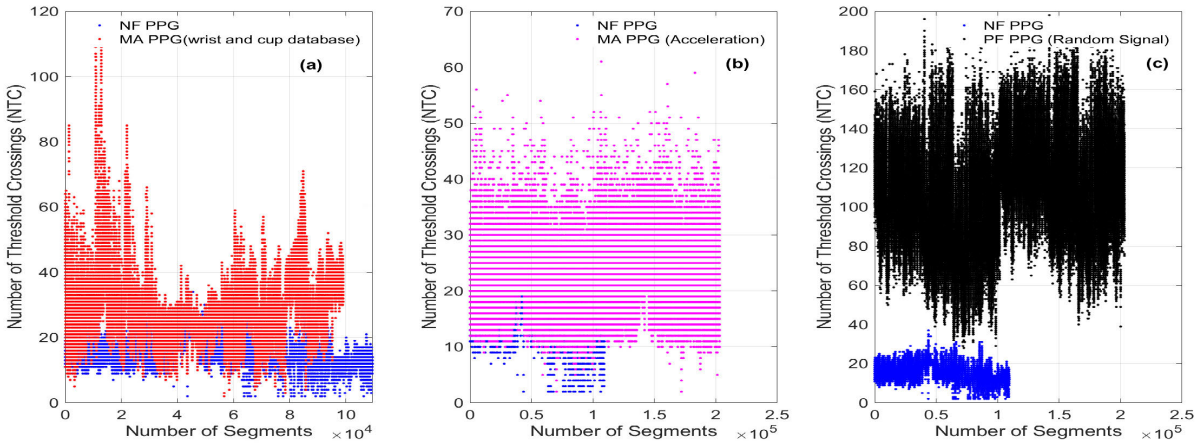

FIGURE 4. Estimated number of threshold crossings (NTC) from (a) noise-free PPG signals and movement artifact corrupted PPG signals taken from the wrist and cup databases, (b) noise-free PPG signals and movement corrupted PPG signals created using the acceleration signals with different levels and (c) noise-free PPG signals and noisy PPG signals created using additive white noises with different amplitude levels.

signals, while in noise-free PPG segments, the respective NZC values are generally lower. For the large amplitude baseline drifted PPG signal, the NZC can be nearly 1 or 2. The presence of very low-amplitude HF noises can often cause severe jitters around zero-crossing points of the zero-mean PPG signal. Therefore, a number of threshold-crossings (NTC) are computed with a predefined threshold λ_{NTC}, in order to reduce very small amplitude noises which can be smoothed out using time-domain filters. The NTC represents the number of times the signal amplitude crosses a reference positive threshold line. The NTC is computed as

$$\text{NTC} = \sum_{n=0}^{N-1} \frac{|\text{sign}\{x[n] - \lambda_{NTC}\} - \text{sign}\{x[n-1] - \lambda_{NTC}\}|}{2}, \tag{20}$$

where sign$\{x\}$ returns $+1$ when $x \geq 1$ and -1 otherwise. The zero-mean PPG signal contains two threshold-crossings for upward-systolic and downward-diastolic slopes. In addition to slope threshold crossings, the prominent dicrotic-diastolic portion results in two threshold crossings. Thus, each cycle of the zero-mean PPG signal can contain 2-4 threshold crossings. For 2 second PPG signal, the maximum number of pulse cycles maybe 10 for a refractory period of 200 ms (i.e., 300 bpm). The minimum number of cycles may be 1 (i.e., 30 bpm). For a 5 second signal, the NTC value may vary from 10 to 100 for pulse intervals of 2000 ms to 200 ms, respectively. Fig. 4 estimated the number of threshold crossings (NTC) from (*i*) noise-free PPG signals, (*ii*) movement artifact corrupted PPG signals taken from the wrist and cup databases, (*iii*) movement corrupted PPG signals created using the acceleration signals with different levels and (*iv*) noisy PPG signals created using additive white noises with different amplitude levels. Preliminary results of this study showed that the number of threshold crossings (NTC) can be used to detect pulse-free noisy signals (i.e., encountered when the sensor is disconnected from the measurement site) and noisy PPG signals. The NTC feature is used as the first decision rule of the SQA algorithm because of its simplicity in the computation as compared to the other time-domain features which are described in the following subsections. Based on the lower and upper bounds of NTC as shown in Fig. 4, noisy PPG signals corrupted with very low-frequency and high-frequency noises can be detected by selecting a suitable NTC threshold value.

3) ON-WIDTH AND OFF-WIDTH DURATION FEATURES FROM THRESHOLDED PREDICTION ERROR SIGNAL

In this paper, we present minimum on-width and off-width durations, maximum on-width and off-width durations, and their counts that are computed from the gate waveform which is obtained by applying the amplitude thresholding rule with a predefined threshold. In this study, amplitude thresholds of 0.1, 0.15, and 0.2 are considered to obtain the best signal quality assessment results. The detection rules which are used are summarized below:

- **Rule01:** Minimum on-width (countpwonmin) and minimum off-width (countpwoffmin) duration must be greater than 100 ms. Count the number of cycles if not satisfied Rule01.
- **Rule02:** Maximum on-width (countpwonmax) and maximum off-width (countpwoffmax) duration must be less than 2.5 sec. Count the number of cycles if not satisfied Rule02.
- **Rule03:** All on-width (countpwon) should lie between 20% of the mean of all on-widths. Count the number of cycles if not satisfied Rule03
- **Rule04:** All off-width (countpwoff) should lie between 20% of the mean of all off-widths. Count the number of cycles if not satisfied Rule04.

- **Rule05:** All on+off width (countpwonoff) should lie between 20% of the mean of all on+off widths. Count the number of cycles if not satisfied Rule05.
- **Rule06:** First order predictor coefficient (FOPC) value.

The algorithm for signal quality assessment (SQA) is presented below (Pseudocode II-A3) based on four time-domain features such as the number of threshold crossings (NTC), maximum and minimum amplitudes, on-width and off-width durations and first-order predictor coefficient (α).

Pseudocode II-A3: Rules for SQA Method

Step-01: Sensor's disconnection and PPG signal with very low-frequency movements and high-frequency noises.
if((NTC $<$ 5 || NTC$>$75)) **then**
signal=0; "*Unacceptable*"
else then
Step-02: Sensor's disconnection with very low-frequency movements and low-amplitude noises, and high-frequency noises.
if (maxAmp$<$1.2*minAmp) **then**
signal=0; "*Unacceptable*"
else then
Step-03: Noisy PPGs corrupted with non-periodic motion artifacts
if(α $<$ 0.980) **then**
signal=0; "*Unacceptable*"
else then
Step-04: Noisy PPGs corrupted with motion artifacts
if(countpwonmax$>$0 || countpwoffmax$>$0) **then**
signal=0; "*Unacceptable*"
else then
if((countpwonmin$>$ c_{th} || countpwoffmin$>$ c_{th}) **then**
signal=0; "*Unacceptable*"
else then
if(countpwon$>$ c_{th}) **then**
signal=0; "*Unacceptable*"
else then
if(countpwoff$>$ c_{th}) **then**
signal=0; "*Unacceptable*"
else **then**
if(countpwonoff$>$ c_{th}) **then**
signal=0; "*Unacceptable*"
else then
signal=1; "*Acceptable*"
endif
endif
endif
endif
endif
endif
endif
endif

In the proposed SQA method, on-width and off-width durations are computed from the smoothed quantized prediction error signal which is the intermediate result of the predictive coding-based data compression method which will be presented in the next subsection.

B. PREDICTIVE CODING BASED PPG COMPRESSION

Fig. 5 depicts a simplified block diagram of predictive coding-based PPG data compression and decompression with integrated onset-systolic peak detection. The predictive coding-based data compression method consists of differential pulse code modulation (DPCM) architecture for compression, prediction error signal-based onset-systolic peak determination with smoothing filter and positive and negative zero crossing detection; and the DPCM decoding architecture includes the DPCM decoder for the reconstruction of the PPG signal from the received binary sequence. For the PPG signal $x[n]$ and the predicted signal $\hat{x}[n]$ with the first-order predictor coefficient $\alpha_1^{(1)}$, the prediction error signal can be computed as

$$e[n] = x[n] - \alpha_1^{(1)} * \hat{x}[n], \tag{21}$$

where $e[n]$ is the prediction error. In the predictive coding, the dynamic range of quantized error $e_q[n]$ is very small. Thus, quantized prediction error can be encoded using a less number of bits as compared to the number of bits used for uncompressed digitized data. For the digitized PPG signal with a sampling rate of 125 sample/s and resolution of 10-12 bits, the data rate is 1.25-1.5 kbps. By using linear prediction, the amount of PPG data can be reduced before data transmission or storing with minimal reconstruction error and fewer computational resources.

In this study, we use a predictor order of 1 for automatically detecting the systolic peaks of the PPG signal by processing the prediction error signal which is the output of the data compression stage. The compression performance of the method is investigated for different lengths of the quantization codebook. For the PPG signal as shown in Fig. 6(a), the quantized prediction error signal is shown in Fig. 6(b). The original PPG signal can be reconstructed by using the predictor coefficient, quantized error signal, and adder. The reconstructed or decoded signal is shown in Fig. 6(c). From the compression and decompression results, it is observed that the reconstructed signal includes discontinuities and quantization noise. In order to reduce the effect of the spurious noises introduced by the quantization process, the reconstructed signal is processed using the moving average filter with a length of 4 samples. The output waveform of this filter is shown in Fig. 6(d). The error between the original and reconstructed signals is shown in Fig. 6(e) for visually evaluating both global and local waveform distortion.

In past studies, different signal processing techniques were used for compression, signal quality checking or artifact presence detection, and onset-systolic peak detection. For example, the compression was performed using the discrete cosine transform (DCT) with coefficient thresholding and/or quantization at the sensing node and then onset-peak detection requires the reconstruction of the PPG signal using the inverse DCT. In DCT-based data compression, there is a possibility of determining the pulse rate by processing

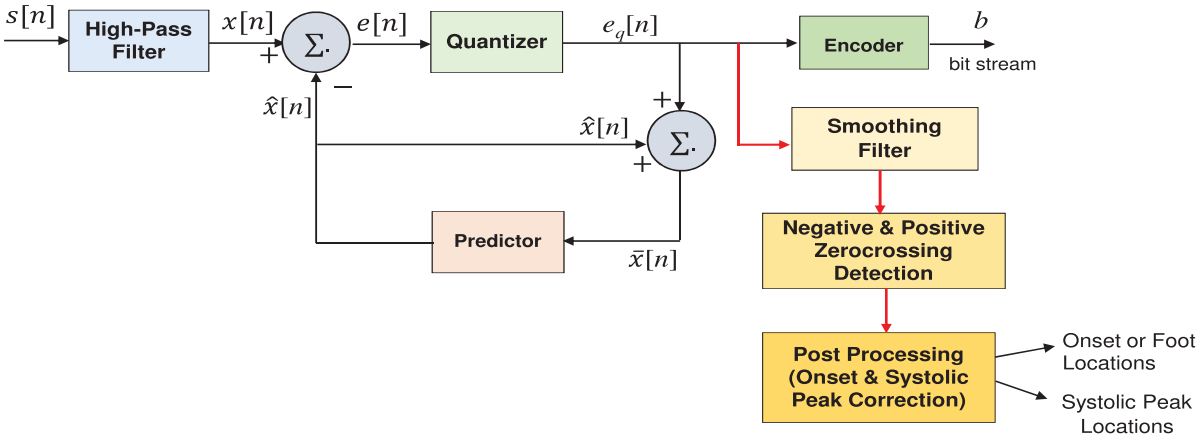

(a) DPCM Based Compression Structure with Onset & Systolic Peak Point Determination

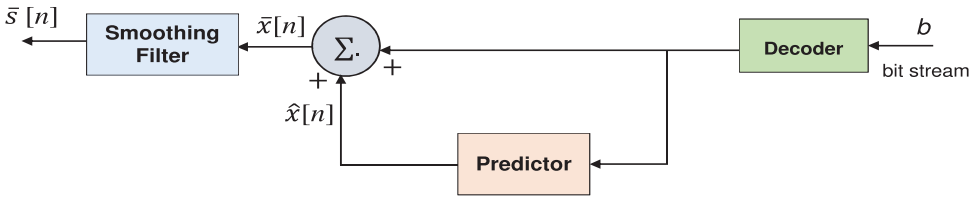

(b) DPCM Based Decompression Structure

FIGURE 5. Block diagram of predictive coding based PPG data compression and decompression with the integrated onset and systolic peak determination by processing the quantized prediction error.

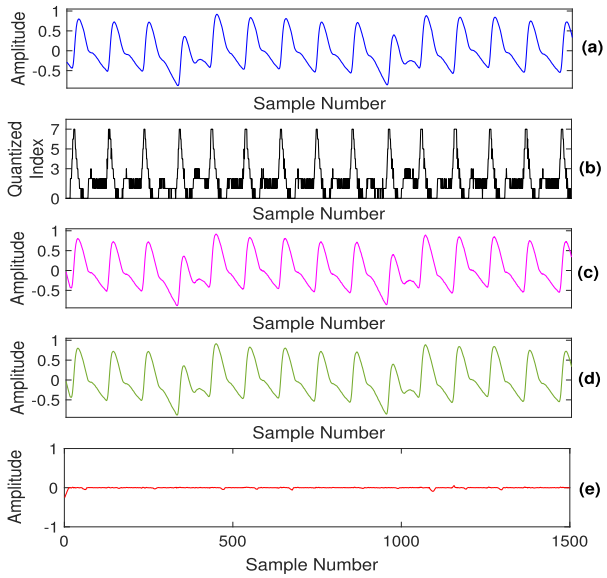

FIGURE 6. Results of predictive coding: (a) Original PPG signal, (b) Quantized prediction error, (c) Decoded signal, (d) Smoothed reconstructed signal, (e) Error signal.

the DCT coefficients at the cost of computational resources and processing time. The accurate pulse rate estimation may be difficult in the transformed domain under different kinds of PPG morphological patterns. Thus, for transform-based PPG data compression, decompression is essential for determining onsets and systolic peaks of the PPG signal that is always performed at the receiver side or off-line processing applications. Otherwise, there is a need for an additional signal processing task for onset-systolic peak detection which is mostly performed by using the time-domain derivatives. In continuous parameter extraction scenarios, signal derivative operation incurs a significant amount of energy consumption in addition to the energy consumption of the decompression process with additional requirements of computational resources. Various onset and/or peak detection methods were proposed by using different kinds of digital filters, derivatives, and signal decomposition techniques [31], [32], [33] but the real-time implementation and energy consumption analysis was not addressed by considering the resource-constrained devices. In this paper, we explore the PR and RR measurement by detecting onset-systolic peak points by processing the quantized prediction error signal of the predictive coding as shown in Fig. 5.

C. PREDICTION ERROR BASED ONSET-SYSTOLIC PEAK DETECTION

Exploring a lightweight and automatic accurate onset-systolic peak detection is highly demanded accurate measurement of PR and RR parameters from the PPG

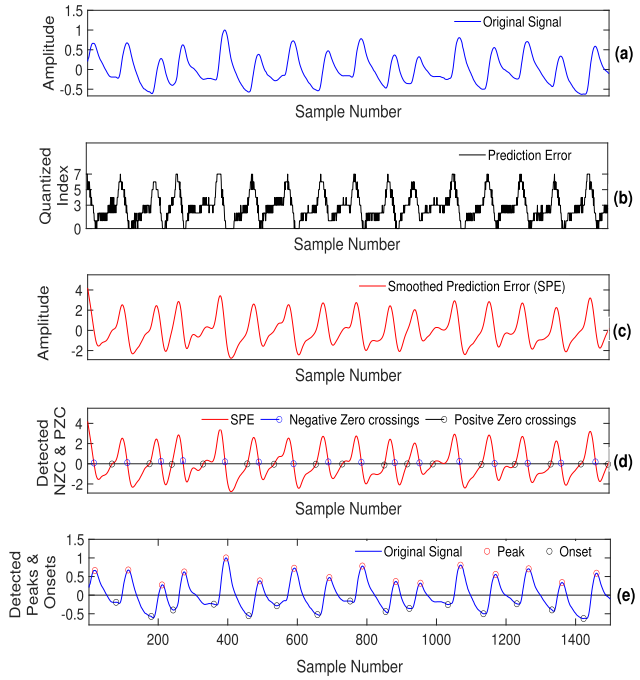

FIGURE 7. **Prediction error based onset-systolic peak detection: (a) Original PPG signal(b) Quantized prediction error, (c) Smoothed prediction error, (d) Detected negative zero crossing points and positive zero crossing points, (e) PPG signal with detected systolic peaks and onsets.**

signal [28], [34]. This study attempts to present a lightweight unified predictive coding framework to jointly perform quality-aware data compression and onset-systolic peak determination as shown in Fig. 5. In the predictive coding-based compression method, the quantized prediction error signal (in Fig. 7(b)) can be directly processed to detect the onset and systolic peak points of the PPG signal. In order to reduce the step-like discontinuity in the quantized prediction error signal as shown in Fig. 7(b), smoothing is performed by using the M-point moving average filter which is defined as:

$$\hat{s}[n] = \frac{1}{M}\sum_{m=0}^{M-1} e_q[n-m]. \tag{22}$$

In this study, the moving averaging filter length is fixed to 5 samples. The output of the smoothing filter is shown in Fig. 7(c). From the result, it can be observed that the positive zero crossing (PZC) point corresponds to the onset, and the negative zero crossing (NZC) point corresponds to the systolic peak of the PPG signal. By processing the prediction error which is available at the sensor node, onsets and systolic peaks can be determined without performing reconstruction of the original signal from the quantized prediction error signal. Therefore, the negative zero crossing (NZC) and positive zero crossing (PZC) points are determined for the smoothed quantized prediction error signal that is used as the candidate points to accurately locate the systolic peaks and onsets. The predictive coding-based onset-systolic peak detection algorithm is summarized below (Pseudocode III-C):

Pseudocode III-C: Peak-Onset Detection

Input: $x[n]$:= PPG signal; $n = 1, 2, \ldots.., L$
Output: SP= Systolic peak location and ONSET= Onset location
Step0: Acquire the PPG signal $x[n]$.
Step1: Normalization: $y[n] = \frac{x[n]}{\max(abs(x[n]))}$
Step2: Obtain the prediction error using Levinson Durbin algorithm
$e(n) = y(n) - \alpha y(n-k)$, where α = prediction coefficient
Step3: Perform smoothing using moving average filter
$y[n] = \frac{1}{P}\sum_{k=0}^{P-1} e[n+k]$
Step4: Detect negative zerocrossing (nzcr1) and positive zero-crossing (pzcr1) of the smoothed PE
if $y(n+1) * y(n) < 0$ and $y(n+1) - y(n) < 0$ **then**
NLoc=n;
endif
if $y(n+1) * y(n) < 0$ and $y(n+1) - y(n) > 0$ **then**
PLoc=p;
endif
Step5: Apply post processing to detect true systolic peaks and onsets
Rule 01: nzcr2=NLoc(find(y(nLoc)>0))
Rule 02: pzcr2=PLoc(find(y(PLoc)<0))
Rule 03: exsp=0; RspT=[]; onsetT=pzcr2;
for i=3:length(nzcr2) **do**
if y(nzcr2(i)) < 0.25*y(nzcr2(i-1)) **then**
RspT=[RspT;i];
exsp=exsp+1;
nzcr2(i)=nzcr2(i-1);
y(nzcr2(i))=y(nzcr2(i));
endif
endfor
SP = unique(nzcr2,'first');
if(exsp>=1)
RonsetTL=RspT-1;
RonsetT=onsetT(RonsetTL);
for k=1:length(RonsetT)
onset=onsetT(onsetT=RonsetT(k));
endfor
endif
endprocedure

The effectiveness of the proposed onset-systolic peak detection method is shown in Figs. 7 and 8 for the PPG signals to have time-varying peak amplitudes, waveform shapes, and pulse-to-pulse intervals. From the detection results of Fig. 7, onset-systolic peak locations can be determined accurately by processing the negative zero-crossing point and positive zero-crossing point of the smoothed prediction error signal. The post-processing is presented with simple detection rules to eliminate the noise peaks and diastolic peak points with a duration threshold measured between the positive zero-

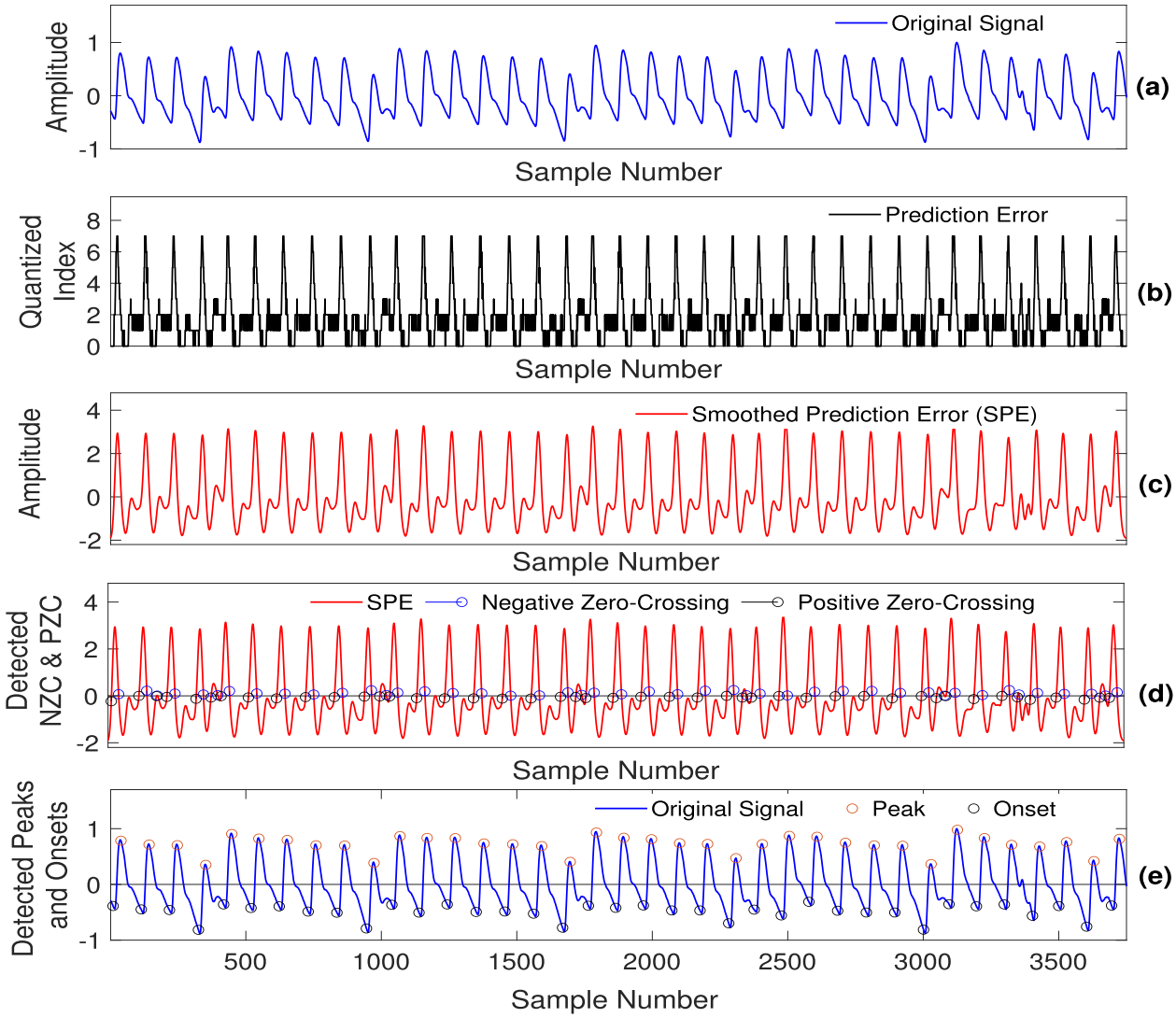

FIGURE 8. Prediction error based onset-systolic peak detection: (a) Original PPG signal(b) Quantized prediction error, (c) Smoothed prediction error, (d) Detected negative zero crossing points and positive zero crossing points, (e) PPG signal with detected systolic peaks and onsets.

crosssing point and negative thresholding point. Fig. 8 shows onset-systolic peak detection results for longer-duration PPG signal having different peak amplitudes.

D. PREDICTIVE CODING BASED PR ESTIMATION METHOD

In this paper, the prediction error (PE) and amplitude threshold (ATh) based PR estimation methods are presented with post-processing rules to reduce the number of false positives due to the prominent tidal and diastolic peaks. The PR estimation performances are compared with existing PR estimation methods such as fast Fourier transform (FFT), autoregressive (AR), and the autocorrelation function (ACF). The algorithms of FFT-based, AR-based (Yule-Walker (YW)-based), ACF-based, and ATh-based PR estimation algorithms are described in Pseudocode III-D that are widely used in most of the commercial vital sign monitoring devices [35], [36], [37].

In this study, the amplitude threshold (ATh)-based PR estimation method is presented by estimating the average PPIs and the number of systolic peaks which are determined by using the amplitude thresholding rule on the uncompressed PPG signal. Two amplitude thresholds (th = 0.15 and th = 0.2) were considered for performance evaluation. The simple post-processing rule to reject false positives. The predictive coding-based PR estimation method is presented based on the onset and systolic peak detection method reported in this paper. For ATh-based and predictive coding-based PR estimation methods, the pulse rate is computed in two ways: (1) PR = NSP × NB, where NB is the number of blocks/minute, NSP denotes the number of systolic peaks in the block and (2) PR $= \frac{F_s}{\text{PPI}_{\text{avg}}} \times 60$ (in bpm), wherein PPI_{avg} is the average of the PPIs within the block duration. In the spectrum-based methods, the frequency resolution, $\Delta f = \frac{\text{Fs}}{\text{NFFT}}$, affects the measurement accuracy in terms of

Pseudocode III-D: PR Estimation Algorithms

procedure [PR]=PRestimation (x, L, Fs)
Input: $x[n]$:= PPG signal; $n = 0, 1, 2, \ldots., L-1$ and
Output: PR(in bpm)
Step0: Collect the PPG data $x[n]$.
Step1: Perform high-pass filtering using 3rd order Chebyshev Type-1 with a cut-off frequency of 0.5 Hz and passband ripple of 0.1 to remove baseline wanders,
$[b, a] = \text{cheby1}(3, 0.1, \frac{0.5\times2}{F_s}$, 'high');
$y[n]$=filtfilt(b, a, $x[n]$);
Perform Amplitude Normalization: y[n] $= \frac{\text{y[n]}}{\max(\text{abs(y[n])})}$
—Fourier Magnitude Based PR Estimation Method—
Step2: Find FFT, Y[k] = fft($y[n]$, N), N $= 2^{\text{nextpow2}(L)}$
Step3: Find Fourier magnitude spectrum, $|Y[k]| = \text{abs}(Y[k])$
Step4: Find the maximum spectral value ($k_{\max}$) between 0.5 to 5 Hz
Step5: Find the PR $= \frac{k_{\max} * F_s}{N} \times 60$ (in bpm)
endprocedure
—Autocorrelation (AC) Based PR Estimation Method—
Step2: Find AC, $R[l] = \frac{\sum_{n=0}^{L-1-l} y[n]y[n+l]}{\sum_{n=0}^{L-1} y^2[n]}$, $l = 0, 1, ..L-1$
Step3: Determine consecutive negative threshold crossing points of $R[l]$ with a threshold of 0.15
if $(R[l] > th)$ && $(R[l+1] < th)$
ntcr1=i; and ntcr=[ntcr;ntcr1];
endif
L_{max} = ntcr(2) − ntcr(1);
Step4: Find the PR $= \frac{F_s}{L_{max}} \times 60$ (in bpm)
endprocedure
—Autoregressive (AR) Based PR Estimation Method—
Step2: Find power spectral density using Yule-Walker's method
$[Py, F] = \text{pyulear(y[n], order, N, Fs)}$;
order=100; $N = 2^{\text{nextpow2}(L)}$;
F_s=sampling frequency
Step3: Determine the maximum spectral value (k_{max}) between 0.5 to 5 Hz
Step4: Find the PR $= \frac{\text{k}_{\max} * \text{Fs}}{\text{N}} \times 60$ (in bpm)
endprocedure
—Amplitude Threshold (ATh) Based PR Estimation Method—
Step2: Perform the amplitude thresholding
$y_p[n] = \begin{cases} 1 & y[n] > th \\ -1 & y[n] < th \end{cases}$
Step3: Determine negative zero-crossing (nzcr1) and positive zero-crossing (pzcr1) points on the $y_p[n]$
if $y_p[n+1] * y_p[n] < 0$ and $y_p[n+1] - y_p[n] > 0$
then pzcr=n;
endif
if $y_p[n+1] * y_p[n] < 0$ and $y_p[n+1] - y_p[n] < 0$
then nzcr=n;
endif
Step4: Determine the location of systolic peak (SPL)
spl = max(xbo(pzcr(i) : nzcr(i))) = pzcr(i) + spl − 1;
Step5: Perform post-processing to detect true systolic peak (SP)
Rule 01: $nzcr2 = PLoc(find(y(PLoc) > 0))$
Rule 02: **for** i=3:length(nzcr2) **do**
if $y(nzcr2(i)) < 0.25 * y(nzcr2(i-1))$
then nzcr2(i)=nzcr2(i-1);
y(nzcr2(i))=y(nzcr2(i));
endif
endfor
SP = unique(nzcr2, 'first');
Step6: Find the average pulse-to-pulse interval (PPI)
for i=2:length(SP) **do**
PP(i-1)=SP(i)-SP(i-1)
endfor
PPI_{avg}=mean(PP)
Step7: Determine the total number systolic peaks (NSP)
Step8: Find the PR (in two ways),
(1) PR = NSP × NB,
where NB denotes the number of blocks per minute
or PR $= \frac{\text{NPPI}}{\text{BD}} \times 60$,
where NPPI denotes the number of PPIs;
BD denotes Block Duration
(2)PR $= \frac{F_s}{\text{PPI}_{\text{avg}}} \times 60$ (in bpm)
endprocedure

beat resolution. The FFT-based methods used the number of data points (NFFT) of 8192 [35] and 1024 [36]. The AR-PSD based PR estimation method used the order of 4 [37]. For example, for $F_s = 125$ Hz, the beat resolution (BR) is 3.66 beats for a 10 s PPG data with 2048 FFT points, and the BR is 0.9155 beats for a 60 s PPG data with 8192 FFT points. Similarly, for $F_s = 25$ Hz, the beat resolutions are 5.85 beats and 0.73 beats for 10 s (NFFT = 256) and 60 s (NFFT = 2048), respectively. Thus, the estimation error can be reduced with a suitable signal length or the NFFT points by considering the power consumption and processor speed of devices. In this study, the NFFT is fixed to the next power of 2 that is larger than the input length $L = D \times F_s$. In this study, we investigate the performance of seven PR estimation methods based on the Fourier magnitude, autocorrelation, number of systolic peaks, and average PPI.

E. PREDICTIVE CODING BASED RR ESTIMATION METHOD

In the PPG signal, the pulsatile component is superimposed on the non-pulsatile component which may contain slowly varying baseline components due to the respiration, sympathetic nervous system activity and thermoregulation [38]. The DC component varies slowly with respiration, vasomotor activity, and thermoregulation. During respiration, the PPG signal is modulated by several physiological factors in its amplitude (stroke volume decreases or increases), baseline (small decrease or increase in central venous pressure increasing venous return), and frequency (heart rate increase or decrease) [39]. Therefore, many researchers have attempted to extract respiratory signals from PPG signals by exploring amplitude modulation (AM), baseline wandering (BW), frequency modulation (FM), and digital frequency-selective filter with a cut-off frequency of respiratory frequency range. It was observed that the respiratory modulations of PPG signals differ in strength based on different physiological mechanisms [40].

The estimation of respiratory rate (RR, breaths per minute) is mostly performed by analyzing one or more of these modulations. Based on the frequency ranges of heart rate and pulse rate, filtering techniques were explored to distinguish heart and respiratory components from the PPG signal. The cut-off frequency of the respiratory component filter was adopted based on the heart rate [41]. It is difficult to differentiate with a fixed cut-off frequency of filters under exercise conditions [41]. In the power spectra of the PPG signal distinct peaks can be observed that are associated with pulse and respiratory frequency components, respectively, and also spectral peaks of other slower waves [42]. The power spectral density was used to compute the respiratory rate from one or more modulations such as RIIV, RIAV, and RIFV. The pulse rate was computed by using the zero-crossing method and the respiratory rate was computed from the peak interval of the filtered signal [41]. The method had the maximum error of pulse and respiratory rates of 10 beats/min and 7 breaths/min, respectively [43].

Hartmann et al. investigated the difference in the accuracy of PPG-derived respiratory frequency (RF) between measurements from six body sites [finger, wrist under, and upper, forehead, and earlobe] under conditions of normal and deep breathing [39]. It was observed that measurement site and breathing pattern impact the accuracy of PPG-derived RF. The best-recommended measurement sites are the forehead and finger for normal and deep breathing patterns, respectively. Li et al. investigated the correlations between respiratory-induced variations extracted from PPG and simultaneous respiratory signals [44]. Walter Karlen et al. extracted respiratory-induced variations (frequency, intensity, and amplitude) from the PPG using the Incremental-Merge Segmentation algorithm and then analyzed the frequency content using fast Fourier transforms [45]. From a clinical point of view, in respiratory rate measurement, over-detection of breaths is more alarming than missed detection [46]. The amplitude of the RIIV signal is related to the respiratory volume [47].

1) RIIV BASED RESPIRATION RATE ESTIMATION METHOD

The respiratory-induced intensive variation (RIIV) introduces a baseline (DC) modulation [47], [48], [49] caused by changes in venous return due to changes in intrathoracic pressure [47], [50]. The small decrease in central venous pressure increases venous return during inspiration and vice-versa. As the venous bed cyclically drains and fills, the baseline is modulated accordingly. The RIIV signal is extracted by using the bandpass filter or the detected systolic peaks of the PPG signal [46]. The heartbeat synchronized and respiratory components can be differentiated with suitable filters for simultaneously estimating heart and respiratory rates [41].

2) RIAV BASED RESPIRATION RATE ESTIMATION METHOD

In the respiratory induced amplitude variation (RIAV), amplitude modulation (AM) caused by left ventricular stroke volume variations due to changes in intra-thoracic pressure [51], [52]. The pulse amplitude is decreased/increased due to a decrease/increase in ventricular stroke volume during inspiration/expiration. In the AM of the PPG signal, systolic peak amplitudes vary over the respiratory cycle.

3) RIFV BASED RESPIRATION RATE ESTIMATION METHOD

In the respiratory induced frequency variation (RIFV), frequency modulation (FM) caused by the respiratory sinus arrhythmia (RSA) wherein pulse rate increases during inspiration and decreases during expiration [51], [52]. The RSA is mainly due to the autonomic regulation of HR during respiration. In the FM of the PPG signal, pulse periods vary over the respiratory cycle [44], [45].

Extraction of the respiration-induced variations (RIIV, RIAV, and RIFV) is presented in Pseudocode III-E. The RR estimation algorithm is presented in Table Pseudocode III-E2 based on the respiration-induced variations (RIIV, RIAV, and RIFV) extracted from the PPG signal by using the onset and systolic peaks detected based on the prediction error as described in this paper. The RR estimation method consists of the following stages: extraction onset and systolic peak detection using the prediction error signal as described in this paper; extracting the respiratory induced variations using the onsets and systolic peaks as presented in Pseudocode III-E; uniform sampling process as presented in Pseudocode III-E1 and estimating respiration rate using the FFT magnitude spectrum as presented in Pseudocode III-E2. Preliminary results of this study are shown in Fig. 9.

Pseudocode III-E: Extract Respiratory Induced Variations From PPG

Input:
[**SP**]:= Systolic peak loaction
[**ASP**] := Amplitude of Systolic peak
[**F**]:= Foot location
[**AF**] := Amplitude of foot
[**Fs**] := Sampling frequency of original PPG signal
Output:
[**RIAV**]:= Respiratory induced amplitude variation
[**RIIV**]:= Respiratory induced amplitude variation
[**RIFVPPI**]:= Respiratory induced frequency variation based on PPI
(pulse-to-pulse interval)
[**RIFVFFI**]:= Respiratory induced frequency variation based on FFI
(foot-to-foot interval)
Step0: Find systolic peak time and its amplitude, onset and its amplitude
Step1: Respiratory induced intensity variation
RIIV=ASP
Step2: Respiratory induced amplitude variation
IA=[];
if $(SP(1) > F(1))$
for k=1:length(SP)
$IA(k) = ASP(k) - AF(k)$;
end
else
for $k = 2 : length(SP) - 1$
$IA(k-1) = ASP(k) - AF(k-1)$;
end
end
RIAV=IA;
Step3: Respiratory induced frequency variation based on PPI
PPI=diff(SP);
RIFV PPI=floor($\frac{Fs*60}{PPI}$);
Step4: Respiratory induced frequency variation based on FFI
FFI=diff(F);
RIFV FFI=floor($\frac{Fs*60}{FFI}$);
end
endprocedure

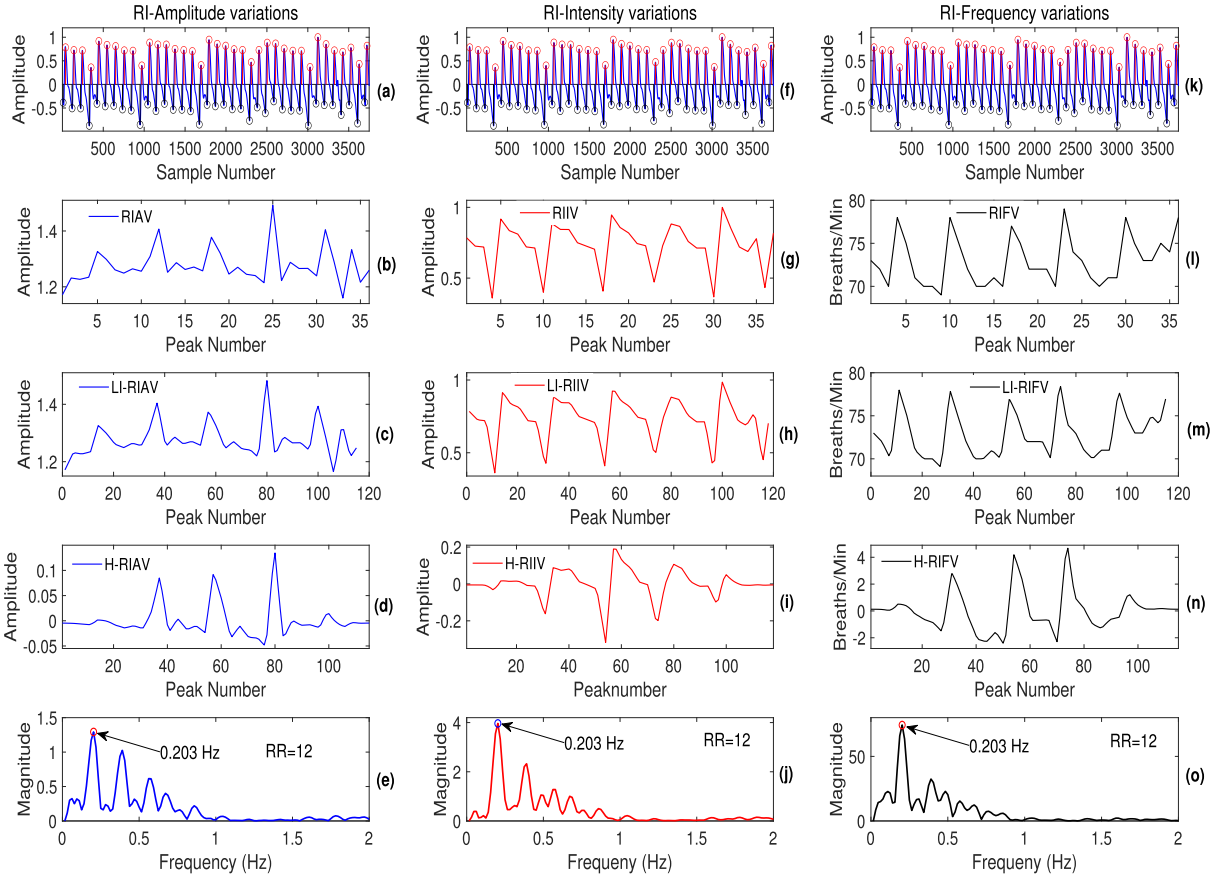

FIGURE 9. RR estimation methods based on the respiratory-induced variations such as respiratory-induced amplitude variation (RIAV), respiratory-induced intensity variation (RIIV), and respiratory-induced frequency variation (RIFV). The waveforms [in (a), (f), and (k)] are the output of predictive coding-based onset-systolic peak detection. The waveforms [in (b), (g), and (l)] are the RIAV, RIIV, and RIFV, respectively. The waveforms [in (c), (h), and (m)] are the outputs of a uniform sampling algorithm. The waveforms [in (d), (i), and (n)] are outputs of windowing. The waveforms [in (e), (j), and (o)] are the FFT magnitude spectrum.

In the estimation results as shown in Fig. 9, the waveforms [in (a), (f) and (k)] are the output of predictive coding based onset-systolic peak detection; the waveforms [in (b), (g) and (l)] are the extracted respiratory-induced amplitude variation (RIAV), respiratory-induced intensity variation (RIIV), respiratory-induced frequency variation (RIFV), respectively; the waveforms [in (c), (h) and (m)] are the outputs of uniform sampling algorithm which is performed before estimating RR from the respiratory induced variations; the waveforms [in (d), (i) and (n)] are outputs of windowing which is performed to reduce the spectral leakage due to the discontinuity at the boundary of the respiratory-induced variation sequence; and waveforms [in (e), (j) and (o)] are the FFT magnitude spectrum with detected dominant spectral peak which is used to estimate the respiration rate.

IV. RESULTS AND DISCUSSION

In this section, we present the evaluation results of each stage of the proposed unified quality-aware PR-RR parameter extraction, compression, and transmission which are tested using the standard databases and performance metrics.

A. PERFORMANCE METRICS

From the detection results, the following parameters are computed: true positive (TP) when it is correctly detected the positive class (noise-free segments), false negative (FN) when it is not detected the negative class, false positive (FP) when it is falsely detected the positive class and true negative (TN) when it is correctly detected the negative class (noisy segments). By using these quantitative parameters, we used the following benchmark metrics such as sensitivity (Se), and false alarm reduction rate (FARR).

In this study, detection accuracy is computed by comparing with expert beat-beat annotations provided in the standard database for algorithm validation. A beat-to-beat comparison between reference annotation and method output is performed to assess the performance of the method. The systolic peaks and onsets are considered to match if they are within an acceptance interval of 20 ms. By comparing the manual annotations with the method-based annotations, the TPs, FPs, TNs and FNs are computed for each of the PPG signals.

We used the standard performance metrics such as mean absolute error (MAE), Pearson correlation coefficient (PCC), Bland and Altman plots, and statistics such as bias, standard

Pseudocode III-E1: Perform Uniform Sampling of RIV Sequence

procedure [xus,tus]=linearinterpolation(x,n,Fs,Fsr)
Input:
[**x**]:= Induced variations RIAV,RIIV,RIFV
[**n**] := Number of samples
[**Fs**] := Sampling frequency of original PPG signal
[**Fsr**] := Required uniform sampling frequency of Induced variations
Output:
[**xus**]:= Induced variations RIAV,RIIV,RIFV after uniform sampling
[**tus**] := Timing instants after uniform sampling
Step0: Acquire the respiratory-induced variations RIAV,RIIV,RIFV
Step1: Passed through liner interpolator
if(length(x)==length(n))
$t = \frac{n.}{Fs}$;
$tus = t(1) : \frac{1}{Fsr} : t(end)$;
xus=interp1(t,x,tus,'*linear*');
else
d=abs(length(x)-length(n));
$t = \frac{n(1:end-d).}{Fs}$;
$tus = t(1) : \frac{1}{Fsr} : t(end)$;
xus=interp1(t,x,tus,'*linear*');
end
endprocedure

Pseudocode III-E2: RR Estimation Using RIVs and FFT Spectrum

procedure [RR]=RRestimationRIVFFT(x, L, Fs)
Input: $x[n]$:= PPG signal; $n = 1, 2, \ldots.., L$ and
Output: RR(in bpm)
Step0: Acquire the PPG signal $x[n]$**.** and subtract mean form the signal
x=x-mean(x);
Step1: Find Systolic peak, the amplitude of systolic peak, foot, and amplitude of foot
Step2: Extract uniform sampled Respiratory induced variations RIAV,RIIV, RIFV PPI and RIFV FFI by using Pseudocode III-E and III-E1
Step3: Passed through Hamming window and subtract mean
RIVh=RIV.*hann(length(RIAV))';
RIVh=RAVh-mean(RIVh);
Step4: Compute FFT, Y[k] = fft($RIVh[n]$, NFFT), $\text{NFFT} = 2^{\text{nextpow2}(L)}$
Step5: Compute magnitude spectrum, $|Y[K]| = \text{abs}(Y[K])$
Step6: Find the local spectral maximum ($k_{\max}$) between 0.1 Hz to 1 Hz
Step7: Compute the RR = $\frac{k_{\max} * F_s}{N} \times 60$ (in bpm)
endprocedure

deviation (SD), limits of agreement (LOA), and Bland-Altman ratio (BAR) were used to estimate a level of agreement between the actual and estimated PR values [55].

$$\text{PCC} = \frac{\sum_{i=1}^{P}(x_i - \bar{x})(y_i - \bar{y})}{\sqrt{\sum_{i=1}^{P}(x_i - \bar{x})^2 \sum_{i=1}^{P}(y_i - \bar{y})^2}}, \tag{23}$$

$$\text{Bias} = \frac{1}{n}\sum_{i=1}^{P}(y_i - x_i), \tag{24}$$

$$\text{SD} = \sqrt{\frac{1}{P-1}\sum_{i=1}^{P}(y_i - x_i - \text{Bias})^2}, \tag{25}$$

$$(\text{LOA}) = \text{Bias} \pm 1.96\ \text{SD}, \tag{26}$$

$$\text{BAR} = \frac{1.96\ \text{SD}}{\frac{1}{P}\sum_{i=1}^{P}\frac{y_i + x_i}{2}}. \tag{27}$$

In past studies, absolute error (AE) was used to find the difference between the reference and derived respiration rate (RR). The AE metric is computed as:

$$AE_i = |RR_{ref}(i) - RR_{est}(i)|, \tag{28}$$

where $RR_{ref}(i)$ denotes the RR of the original respiratory signal and $RR_{est}(i)$ denotes the RR of the extracted respiratory signal for i^{th} observation. The mean absolute error (MAE) was used to assess the performance of the estimation methods [10]

$$\text{MAE} = \frac{1}{P}\sum_{i=1}^{P} AE_i \tag{29}$$

where P denotes the number of PRs.

B. PERFORMANCE OF PPG SIGNAL QUALITY ASSESSMENT METHOD

The performance of the proposed SQA method is evaluated in a wide variety of noise-free PPG signals and noisy PPG signals corrupted with motion artifacts having different amplitude levels and also corrupted with additive white Gaussian noises. Finally, real-time implementation of the proposed SQA is demonstrated by using the Arduino Due platform integrated with a pulse sensor, Bluetooth low energy (BLE), and Smartphone devices.

In the SQA method, finding the count threshold is important to achieve a higher sensitivity (Se) and false alarm reduction rate (FARR). Evaluation results are summarized in Table 2 for noise-free (NF) PPG signals and three noisy PPG databases such as (*i*) wrist and cup database, (*ii*) motion-artifact (MA) corrupted PPG databases with different kinds of acceleration signals with different magnitude levels, and (*iii*) noisy PPG database having signals corrupted with random noises with different kinds of magnitude levels. From the results, it is observed that the amplitude threshold of

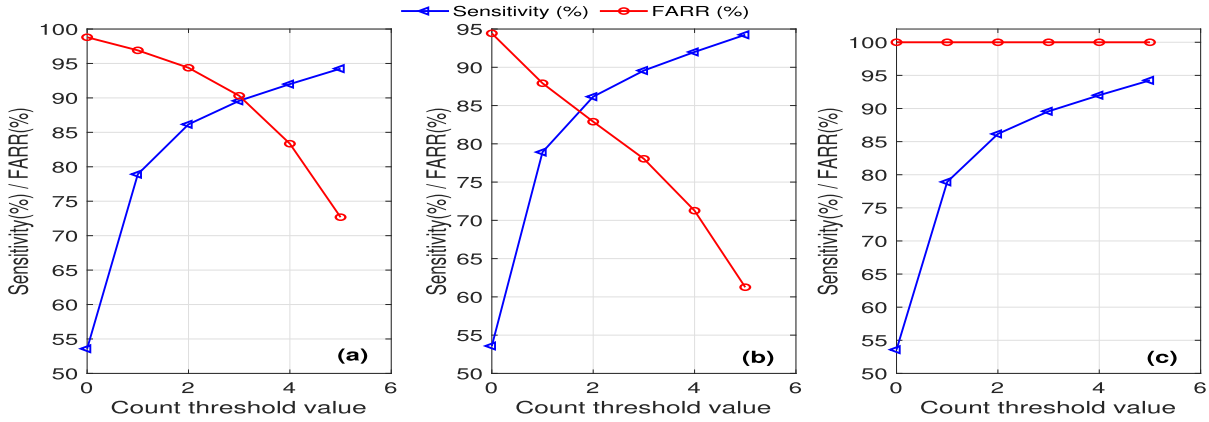

FIGURE 10. Performance of the signal quality assessment method in terms of sensitivity (Se) and false alarm rate reduction (FARR) for (a) noise-free PPG and motion artifact PPG signals from wrist and cup database (b) noise-free PPG and motion artifact PPG signal generated from acceleration signals, and (c) noise-free PPG and random noise signals.

TABLE 2. Performance of signal quality assessment.

Count Value	Th=0.10						Th=0.15						Th=0.20					
	NF PPG vs MA PPG (wrist-cup database)		NF PPG vs MA PPG (Acceleration)		NF PPG vs PF PPG (Random Noise)		NF PPG vs MA PPG (wrist-cup database)		NF PPG vs MA PPG (Acceleration)		NF PPG vs PF PPG (Random Noise)		NF PPG vs MA PPG (wrist-cup database)		NF PPG vs MA PPG (Acceleration)		NF PPG vs PF PPG (Random Noise)	
	Se (%)	FARR (%)	Se (%)	FARR (%)	Se (%)	FARR (%)	Se (%)	FARR (%)	Se (%)	FARR (%)	Se (%)	FARR (%)	Se (%)	FARR (%)	Se (%)	FARR (%)	Se (%)	FARR (%)
<=0	47.28	98.89	47.28	97.11	47.28	100	53.59	98.81	53.59	94.44	53.59	100	56.66	98.38	56.66	91.36	56.66	100
<=1	71.66	96.94	71.66	93.22	71.66	100	78.92	96.90	78.92	87.92	78.92	100	82.14	96.42	82.14	82.28	82.14	100
<=2	78.73	94.72	78.73	90.33	78.73	100	86.16	94.37	86.16	82.89	86.16	100	89.57	92.62	89.57	73.84	89.57	100
<=3	82.28	91.63	82.28	87.46	82.28	100	89.58	90.31	89.58	78.04	89.58	100	93.03	86.47	93.03	65.53	93.03	100
<=4	85.12	86.56	85.12	82.62	85.12	100	92.00	83.35	92.00	71.26	92.00	100	95.23	76.97	95.23	56.22	95.23	100
<=5	87.98	78.36	87.98	74.13	87.98	100	94.25	72.68	94.25	61.26	94.25	100	96.65	64.33	96.65	45.20	96.65	100

0.15 results in better sensitivity and false alarm reduction rate for all the test databases. Fig. 10 shows results for different count thresholds varying from 0 to 5. Achieving higher sensitivity is most important in order to avoid discarding noise-free PPG signals. Based upon this requirement, it can be observed that this method had a Se of 92.00% and FARR of 84.57% for an optimal count threshold of 4. From the evaluation results of different SQA methods which are presented in this paper, it can be observed that the proposed method provides promising quality assessment results in terms of higher sensitivity and false alarm reduction rate as compared to other SQA methods. Further, it can be noted that this method uses width features extracted from the prediction error signal. Therefore, the proposed method can be easily integrated with predictive coding-based data compression and also onset-systolic peak detection methods for discarding the noisy PPG signals from further encoding and parameter extraction processes. Evaluation results demonstrate that on-width and off-width features extracted from the PPG signal or prediction error signal and combined with the first-order predictive coefficient can achieve higher sensitivity and false alarm reduction rate. Moreover, these methods do not demand more computational resources as compared to other methods.

C. PERFORMANCE OF PREDICTIVE CODING BASED COMPRESSION

For investigating the compression performance of predictive coding, quantization codebook lengths of 16, 8, and 4 are considered in this study. For codebook lengths of 16, 8, and 4, the quality of the reconstructed PPG signals is evaluated in terms of percentage root-mean-square difference (PRD), signal-to-noise ratio (SNR), maximum absolute error (MaxAE), normalized MaxAE, wavelet amplitude weighted PRD (WAWPRD), wavelet energy weighted PRD (WEWPRD), mutual information (MI) and Kullback-Leibler Divergence (KLD) [56], [57]. Evaluation results of the proposed compression method are summarized in Table 3. Results demonstrate that the predictive coding-based PPG data compression can achieve compression ratios from 3 to 4 with better reconstruction and minimal error. From the performance study on the objective distortion measures, the

TABLE 3. Performance of predictive coding based PPG compression for different codebook lengths (CL) and signal durations (Dur).

Code book (CL)	Dur (sec)	CR	PRD ($\mu \pm \sigma$)	SNR ($\mu \pm \sigma$)	MaxAE ($\mu \pm \sigma$)	NMaxAE ($\mu \pm \sigma$)	MAE ($\mu \pm \sigma$)	WAWPRD ($\mu \pm \sigma$)	WEWPRD ($\mu \pm \sigma$)	MI ($\mu \pm \sigma$)	KLD ($\mu \pm \sigma$)
16	5	3	1.10±0.55	39.7±3.09	0.026±0.015	0.016±0.008	0.003±0.001	1.64±0.59	0.83±0.58	0.947±0.036	0.240±0.203
	10		1.12±0.46	39.5±3.05	0.033±0.019	0.020±0.010	0.002±0.001	1.71±0.57	0.86±0.58	0.943±0.034	0.066±0.062
	15		1.16±0.49	39.30±3.08	0.0378±0.021	0.0232±0.012	0.0027±0.001	1.76±0.59	0.90±0.56	0.941±0.035	0.040±0.038
	20		1.19±0.50	39.10±3.09	0.0422±0.023	0.025±0.013	0.0027±0.001	1.80±0.59	0.93±0.58	0.940±0.034	0.030±0.030
8	5	4	3.22±1.91	30.67±3.60	0.077±0.036	0.047±0.021	0.0078±0.0050	4.32±1.81	2.71±1.91	0.914±0.049	0.358±0.279
	10		3.33±1.70	30.33±3.53	0.090±0.046	0.055±0.026	0.007±0.0040	4.52±1.76	2.86±1.83	0.910±0.045	0.100±0.080
	15		3.37±1.56	30.16±3.41	0.098±0.045	0.060±0.026	0.0071±0.003	4.60±1.62	2.90±1.65	0.908±0.043	0.062±0.048
	20		3.44±1.59	29.9±3.39	0.106±0.050	0.065±0.029	0.006±0.003	4.71±1.64	2.99±1.68	0.908±0.043	0.046±0.037
4	5	6	9.75±6.26	21.30±3.94	0.168±0.075	0.103±0.042	0.027±0.023	11.80±5.57	8.74±6.46	0.824±0.087	0.464±0.357
	10		10.23±6.72	20.93±4.02	0.191±0.092	0.117±0.051	0.026±0.023	12.41±5.84	9.30±6.79	0.819±0.089	0.165±0.157
	15		10.43±6.89	20.75±3.99	0.204±0.097	0.124±0.054	0.025±0.023	12.68±5.97	9.55±6.94	0.816±0.088	0.110±0.089
	20		10.67±6.94	20.55±4.00	0.217±0.105	0.133±0.058	0.025±0.023	12.96±5.97	9.81±6.97	0.814±0.090	0.090±0.087

pulse rate and respiration rate can be extracted from the reconstructed PPG signals with a PRD value of less than 4%. Although the compression ratio depends on the number of bits used for quantizing the prediction error, compression results of predictive coding for the different signal duration (5, 10, 15, and 20 seconds) are summarized to demonstrate the robustness of the predictive coefficient estimation with time-varying PPG morphologies. It can be observed that the PRD values are nearly the same for all duration cases. Results showed that the distortion varies with codebook length.

Evaluation results showed that the compression performance depends on the codebook length. The CR is increased when the codebook length is smaller at the cost of increased distortion error. Results further showed that the essential PPG waveform features such as slope, systolic peak, tidal, dicrotic notch, and diastolic waves are distorted when the codebook length is smaller. The slope of the systolic portion is highly distorted when the codebook length is 4. From the acceptable distortion metric ranges, it can be noticed that predictive coding results in a compression ratio from 3 to 4 by preserving the fiducial points of the PPG signal. This study suggests that the codebook lengths of 16 and 8 can be more suitable for the compression of PPG signal without distorting essential fiducial points and morphological features. Since the preservation of PPG features is most important, the main consideration must be the perfect PPG signal reconstruction to avoid incorrect measurement of maximum slope, crest time, systolic peak, pulse width, pulse rate, and pulse area.

For visual inspections, outputs of the predictive coding-based data compression and decompression algorithm are shown in Figs. 6 and 11 for different kinds of PPG signals. From the results, it is observed that the PPG signal can be reconstructed with minimal error irrespective of various kinds of pulsatile patterns having varying peak amplitudes and pulse rates. It can be further noticed that dominant peaks and zero-crossing points of the quantized prediction error correspond to the fiducial points of the PPG signal. This is the basis for an integrated or unified framework using predictive coding for jointly performing data compression and onset-peak detection tasks.

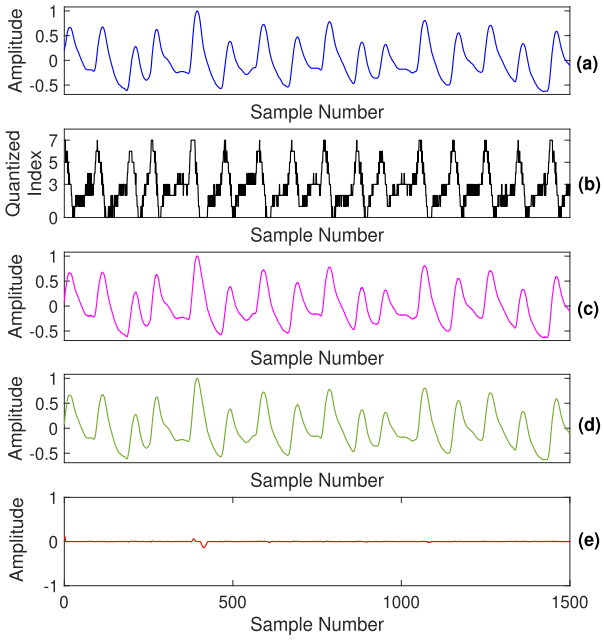

FIGURE 11. Results of predictive coding: (a) Original PPG signal(b) Quantized prediction error, (c) Decoded signal, (d) Smoothed reconstructed signal, (e) Error signal.

D. PERFORMANCE OF PR ESTIMATION METHODS

For performance evaluation, the validation databases (3174 segments, 60 seconds (each)) are created including normal and abnormal PPG signals with a prominent tidal, dicrotic notch and diastolic waves and varying up-stroke and down-stroke waves, normal sinus rhythm, premature atrial con-

traction, ventricle contraction, and atrial fibrillation, regular and irregular rates. We used standard performance metrics such as mean absolute error (MAE), Pearson correlation coefficient (PCC), the Bland and Altman plots and statistics as defined in Section IV-D2, and the computational complexity for evaluating the performance of all PR estimation methods.

1) PERFORMANCE OF THE PR ESTIMATION METHODS UNDER DIFFERENT SAMPLING RATES AND SIGNAL DURATIONS

In this study, we developed existing PR estimation methods based on the Fourier magnitude, autocorrelation, and autoregressive (AR) model, and the other pulse-to-pulse interval (PPI)-based and number of systolic peak (NSP)-based PR estimation methods with estimated systolic peaks and PPIs from the original PPG signal and also smoothed prediction error (PE) signal. The PR estimation methods are summarized below:

- Autocorrelation-based PR estimation method which is performed directly on the original PPG signal as shown in Figs. 12 and 13.
- Fourier magnitude-based PR estimation method which is performed directly on the original PPG signal as shown in Figs. 12 and 13.
- Autoregressive based PR estimation method which is performed directly on the original PPG signal.
- Average pulse-to-pulse interval (PPI) based PR estimation method which is performed directly on the original PPG signal
- Number of systolic peaks (NSP) based PR estimation method which is performed directly on the original PPG signal.
- Average pulse-to-pulse interval (PPI) based RR estimation method which is performed on the smoothed prediction error (PE) signal.
- Number of systolic peaks (NSP) based PR estimation method which is performed on the smoothed prediction error (PE) signal.

For the uncompressed PPG signals with sampling rates (SRs), $F_s = 25$ Hz and $F_s = 125$ Hz, the estimation performances are summarized in Table 4 and Table 5 for seven PR estimation methods for four measurement durations (10 s, 20 s, 30 s and 60 s). For performance comparison, the benchmark metrics such as mean absolute ratio (MAE), Pearson correlation coefficient (PCC) and Bland-Altman ratio (BAR) metrics. For short time periods, final PR in number of beats per minute (bpm) is obtained based on the average calculation approach for the case of ACF- and FFT-based PR estimation methods. In the case of ATh-based and predictive coding-based PR estimation methods, final PR in bpm is computed from a total number of systolic peaks (NSP) or an averaged PPI (PPI_{avg}).

Evaluation results of the PR estimation methods are summarized in Table 4 and Table 5. Estimation results demonstrate that the ATh-based method had the MAE of 0.65, PCC of 0.9962, and BAR of 3.55 with an amplitude threshold of 0.15 and the PR estimation by using the average PPI whereas the PE-based method had the MAE of 0.74, PCC of 0.9968, and BAR of 3.26 with PR estimation by using the average PPI for the 10 seconds uncompressed PPG signal with a sampling rate of 125 Hz that outperforms other three PR estimation methods such as the ACF-based, FFT-based and AR-based methods. For the 20 seconds, uncompressed PPG signal with a sampling rate of 125 Hz, the ATh-based method achieved the MAE of 0.55, PCC of 0.9951, and

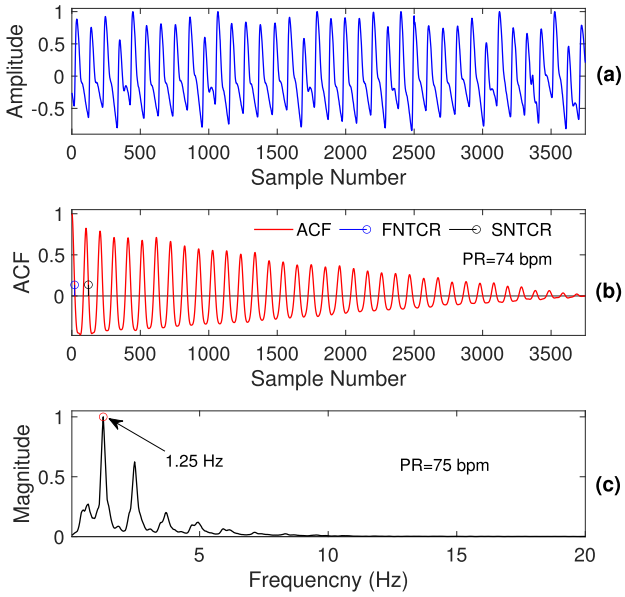

FIGURE 12. Results of PR estimation using the ACF and FFT method: (a) Original PPG signal, (b) Autocorrelation function, and (c) Fourier magnitude spectrum.

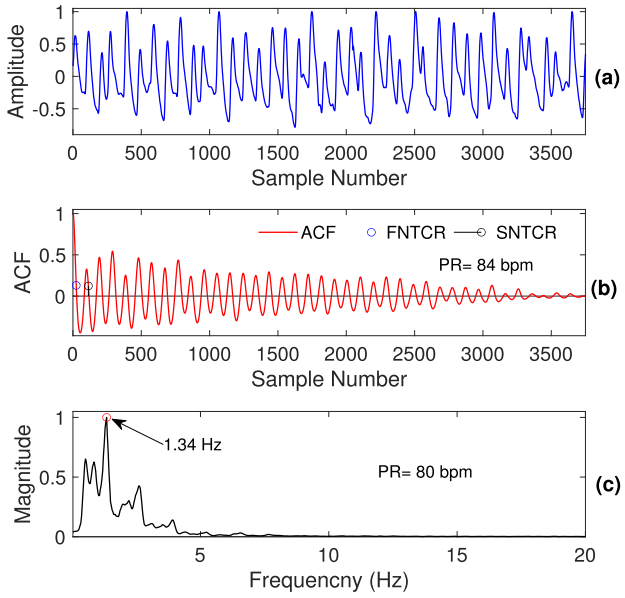

FIGURE 13. Results of PR estimation using the ACF and FFT method: (a) Original PPG signal, (b) Autocorrelation function, and (c) Fourier magnitude spectrum.

TABLE 4. Performance of PR estimation methods in terms of number of segments within estimation error (EE) range (in bpm).

Duration (sec)	Method		SR (Fs) (Hz)	MAE±SD	PCC	BAR (%)	Number of Segments within Estimation Error Range (in bpm)										
							0	1	2	3-4	5-7	8-10	11-15	16-20	21-25	26-30	>30
10	ACF		125	1.52±2.88	0.9842	7.67	1097	1291	346	206	128	43	40	12	8	1	2
			25	2.03±3.62	0.9770	9.59	817	1149	525	348	173	89	40	18	10	2	3
	FFT		125	3.68±5.39	0.9534	12.82	49	220	692	1759	314	66	43	15	3	0	13
			25	6.01±5.48	0.9501	12.91	7	25	52	718	2043	204	63	28	8	11	15
	YULE		125	6.36±12.90	0.8656	29.87	140	411	813	1155	174	50	93	125	65	18	130
			25	11.88±16.30	0.8060	36.57	15	26	68	499	1496	199	127	340	89	80	235
	ATh (0.15)	PPI	125	0.65±1.37	0.9962	3.55	1780	1101	169	89	22	4	5	2	0	1	1
			25	0.84±1.20	0.9967	3.3	1307	1428	291	112	25	4	4	2	0	1	0
		NSP	125	0.80±1.48	0.9954	3.91	1631	1046	315	132	35	5	6	2	0	1	1
			25	1.14±1.37	0.9948	4.2	1014	1335	540	217	52	7	6	2	1	0	0
	ATh (0.20)	PPI	125	0.67±1.50	0.9954	3.88	1805	1091	141	88	32	5	4	6	0	1	1
			25	0.69±1.34	0.9962	3.6	1716	1168	152	88	31	9	5	4	1	0	0
		NSP	125	0.72±1.57	0.9949	4.11	1875	874	248	110	46	8	5	6	0	1	1
			25	1.23±1.60	0.9946	4.2	1036	1243	548	247	72	16	6	5	1	0	0
	PE	PPI	125	0.74±1.19	0.9968	3.26	1559	1228	250	97	32	2	4	1	0	1	0
		NSP		0.96±1.34	0.9955	3.92	1345	1171	397	201	48	6	4	1	0	1	0
20	ACF		125	1.77±4.03	0.9709	10.42	866	1331	497	255	114	33	42	23	3	3	7
			25	2.27±4.08	0.9699	10.9	667	1085	635	433	183	86	50	17	6	6	6
	FFT		125	2.30±5.15	0.9555	12.57	512	1216	720	416	173	81	31	5	5	2	13
			25	3.40±5.40	0.9512	12.9	124	440	904	1212	309	109	46	5	11	0	14
	YULE		125	4.17±12.41	0.8657	29.29	695	1324	551	232	116	45	28	6	22	23	132
			25	7.31±14.96	0.8285	34.4	134	418	776	1053	293	108	49	9	60	85	189
	ATh (0.15)	PPI	125	0.59±1.48	0.9957	3.77	1902	1048	115	67	27	6	6	1	0	0	2
			25	0.68±1.23	0.9967	3.3	1620	1280	163	70	29	5	4	2	0	0	1
		NSP	125	0.57±1.48	0.9957	3.76	2056	831	170	74	29	5	6	1	0	0	2
			25	0.82±1.28	0.9961	3.6	1437	1285	290	108	41	7	3	2	0	1	0
	ATh (0.20)	PPI	125	0.63±1.58	0.9951	4.05	1906	1038	93	85	28	11	4	7	0	1	1
			25	0.64±1.44	0.9958	3.7	1865	1062	106	83	36	10	5	6	0	1	0
		NSP	125	0.55±1.60	0.9951	4.02	2226	664	129	99	35	7	6	6	0	1	1
			25	0.80±1.51	0.9955	3.9	1652	1106	229	104	60	10	8	4	0	1	0
	PE	PPI	125	0.64±1.18	0.9970	3.18	1765	1148	135	80	35	5	4	1	1	0	0
		NSP		0.69±1.24	0.9966	3.37	1791	989	232	109	42	6	3	1	0	1	0

BAR of 4.02 for the PR estimation by using the number of systolic peaks (NSPs) whereas the PE-based method had the MAE of 0.64, PCC of 0.9970, and BAR of 3.18 for the PR estimation by using the average PPI. From the estimation results of Table 5, it is noticed that the ATh-based method achieved the MAE of 0.50, PCC of 0.9959, and BAR of 3.58 with amplitude threshold of 0.15 whereas the PE-based method had the MAE of 0.59, PCC of 0.9969, and BAR of 3.21 with PR estimation by using the number of systolic peaks (NSP) for the 30 seconds uncompressed PPG signal with a sampling rate of 125 Hz that outperforms other estimation methods. For the 60 seconds uncompressed PPG signal with a sampling rate of 125 Hz, the ATh-based method had the MAE of 0.43, PCC of 0.9961, and BAR of 3.59 with an amplitude threshold of 0.15 whereas the PE-based method had the MAE of 0.46, PCC of 0.9972, and BAR of 3.04 with PR estimation by using the number of systolic peaks (NSP). Based on the consideration estimation performance on the three benchmark metrics, it is noticed that the PE-based PR estimation method outperforms other PR estimation methods tested with the same databases with different sampling rates and signal durations.

Evaluation results further showed that the number of systolic peaks (NSP) and average pulse-to-pulse interval (PPI) based PR estimation methods provide accurate PR measurement with less estimation error measured in terms of mean absolute error (MAE), Pearson correlation coefficient (PCC), and Bland-Altman ratio (BAR) metrics for both sampling rates and also for different signal durations. Moreover, onsets and systolic peaks can be detected automatically by processing the prediction error (PE) signal which is the intermediate result of data compression. It is also observed that PE based onset-peak detection method does not require high-frequency component removal as

TABLE 5. Performance of PR estimation methods in terms of number of segments within estimation error (EE) range (in bpm).

Duration (sec)	Method		SR (Fs) (Hz)	MAE±SD	PCC	BAR (%)	Number of Segments within Estimation Error Range (in bpm)										
							0	1	2	3-4	5-7	8-10	11-15	16-20	21-25	26-30	>30
30	ACF		125	1.89±3.52	0.9755	9.45	830	1297	527	273	114	40	42	21	17	7	6
			25	2.57±4.82	0.9585	12.8	589	1018	616	554	203	84	53	18	22	9	8
	FFT		125	2.67±5.40	0.9503	13.34	371	1065	853	462	235	105	56	9	6	0	12
			25	2.36±5.26	0.9520	13.1	586	1262	541	397	219	97	49	8	4	0	11
	YULE		125	5.05±15.34	0.8276	35.87	535	1292	683	257	117	73	36	6	7	1	167
			25	4.30±12.15	0.8623	29.0	531	1161	554	398	248	100	48	19	5	1	109
	ATh (0.15)	PPI	125	0.66±1.44	0.9959	3.70	1697	1238	135	68	22	5	5	2	0	0	2
			25	0.74±1.24	0.9966	3.3	1455	1422	191	70	23	5	5	2	0	0	1
		NSP	125	0.50±1.47	0.9959	3.68	2217	720	128	66	27	7	4	3	0	0	2
			25	0.70±1.33	0.9961	3.6	1644	1223	185	75	29	9	6	2	0	0	1
	ATh (0.20)	PPI	125	0.69±1.54	0.9952	3.98	1700	1221	125	77	30	8	6	5	0	1	1
			25	0.71±1.41	0.9958	3.7	1654	1250	133	83	35	8	5	5	0	0	1
		NSP	125	0.50±1.59	0.9953	3.95	2379	540	107	87	39	8	7	5	0	1	1
			25	0.68±1.54	0.9954	3.9	1909	958	137	96	49	12	6	6	0	0	1
	PE	PPI	125	0.69±1.16	0.9970	3.15	1586	1316	151	81	30	6	2	1	0	1	0
		NSP		0.59±1.21	0.9969	3.21	1964	897	178	89	36	5	3	1	0	1	0
60	ACF		125	2.05±4.22	0.9663	11.09	876	1255	484	295	121	32	34	26	19	15	17
			25	2.90±4.35	0.9610	12.3	479	925	666	622	252	101	55	17	23	14	20
	FFT		125	2.55±5.29	0.9484	13.63	743	1002	472	447	292	142	49	12	5	0	10
			25	2.45±4.79	0.9556	12.6	824	951	466	438	275	142	54	11	5	0	8
	YULE		125	3.65±15.41	0.8044	36.42	1199	1216	266	204	106	59	35	8	8	2	71
			25	3.40±11.15	0.8622	27.1	815	941	422	445	297	129	68	23	4	0	30
	ATh (0.15)	PPI	125	0.55±1.46	0.9959	3.70	2021	940	105	63	30	5	6	2	0	0	2
			25	0.59±1.28	0.9966	3.3	1868	1091	100	71	31	5	6	1	0	0	1
		NSP	125	0.43±1.45	0.9961	3.59	2394	579	95	59	32	6	5	2	0	0	2
			25	0.53±1.28	0.9967	3.3	2053	909	98	69	31	7	5	1	0	0	1
	ATh (0.20)	PPI	125	0.60±1.58	0.9951	4.02	2028	913	95	78	37	9	6	6	0	1	1
			25	0.61±1.48	0.9956	3.8	1980	956	88	87	42	9	5	6	0	0	1
		NSP	125	0.44±1.59	0.9954	3.91	2534	409	88	82	39	8	7	5	0	1	1
			25	0.52±1.50	0.9958	3.7	2297	630	88	94	45	8	5	6	0	0	1
	PE	PPI	125	0.59±1.19	0.9970	3.16	1915	1016	110	88	35	5	3	1	0	1	0
		NSP		0.46±1.20	0.9972	3.04	2292	646	108	79	39	5	3	1	0	1	0

followed at the preprocessing stage of most PR estimation methods. Further, the signal quality assessment based on the predictor coefficient and on-width and off-width durations provides promising results in assessing the quality of PPG signals. Therefore, the predictive coding-based unified framework can reduce overall computational operations.

2) PR ESTIMATION ERROR RANGE ANALYSIS

In the performance evaluation and comparison, a large number of test segments with reference PR values, it can be noticed that the Pearson correlation coefficient may be close to 1 and/or MAE is very small (or <5 bpm). In such a case, the PR estimation method is considered to be good even if the method had a large estimation error for some of the test segments. Further, the BAR value at most 10% is rated as "*good*," and (10% $\leq$ BAR $\leq$ 20%) is rated as "*moderate*," or (BAR $\geq$ 20%) is rated as "*insufficient*" [55]. However, from the visual inspection of the PR estimation error, it can be observed that methods had a large margin of estimation error (in bpm) for some of the test PPG signals. Therefore, evaluation of the PR estimation method in terms of error ranges is essential to highlight the failure cases of the method with respect to the PR values ranging from 30 to 300 bpm that is not been addressed in past studies. In this paper, we present 11 estimation error groups (0, 1, 2, 3-4, 5-7, 8-10, 11-15, 16-20, 21-25, 26-30, >30 bpm) for highlighting the number of segments having a large error margin. Results of this performance study are summarized in Table 4 and Table 5 for different durations of signal and sampling rates. From the estimation error range results for the uncompressed PPG signal with a sampling rate of 125 Hz, it can be observed that the FFT-based PR estimation method achieved the MAE of 2.55 bpm with 76 segments (EE > 10 bpm), 142 segments (EE of 8-10 bpm) and 292 segments (EE of 5-7 bpm) and the ACF-based PR estimation method achieved the MAE of 2.05 bpm with 113 segments (EE > 10 bpm), 32 segments (EE of 8-10 bpm) and 121 segments (EE of 5-7 bpm). The ATh-based PR estimation method achieved the MAE of 0.43 bpm

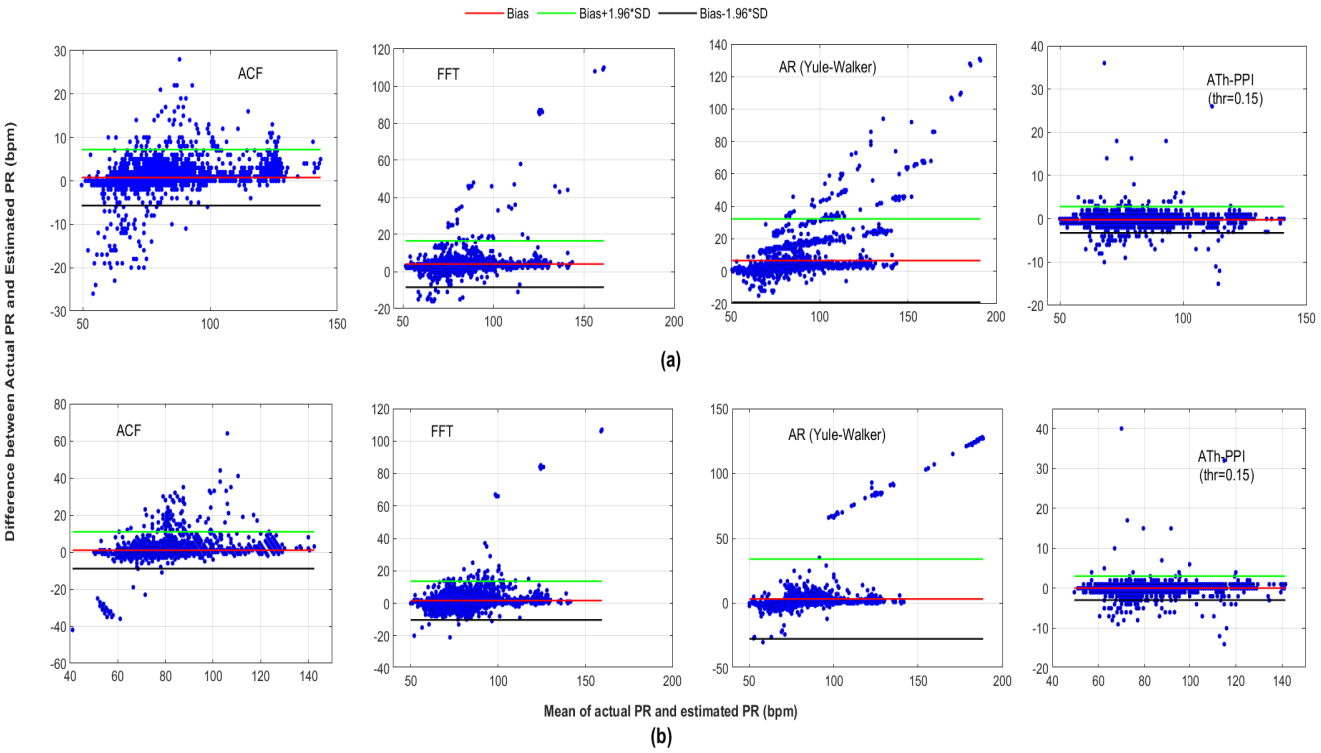

FIGURE 14. Bland-Altman plots for the (a) 10 second and (b) 60 second PPG signal. It shows the differences between the actual and estimated PR measurements with the bias (red line). The 95% upper (green line) and lower (black line) limit of agreement (LOA) with bias of ±1.96 SD, where SD is the standard deviation.

with 9 segments (EE > 10 bpm), 6 segments (EE of 8-10 bpm), and 32 segments (EE of 5-7 bpm) whereas the PE-based PR estimation method achieved the MAE of 0.46 bpm with 5 segments (EE > 10 bpm), 5 segments (EE of 8-10 bpm) and 39 segments (EE of 5-7 bpm) for the PPG signal with a duration of 60 seconds.

The PR estimation error greater than 10 bpm can lead to the wrong diagnosis and would be more problematic in medical settings [58], [59]. From the evaluation results, it can be observed that the FFT-based, ACF-based, and YULE-based methods had more segments with an estimation error of above 10 bpm. Furthermore, these methods had more than 20% segments with an estimation error of above 5 bpm for both sampling rates. From the evaluation results, it is noticed that the PR estimation methods had poor estimation performance when the PPG signals have time-varying pulsatile morphologies and PPIs. Evaluation results show that the Fourier magnitude and AR-based PR estimation methods had a large estimation error due to the aliasing of harmonics of pulse rate with frequency components of prominent tidal and diastolic waves and slopes. Further, the multiplication factor-based PR estimation method had a large error margin for irregular rates. This study further demonstrates that the average PPI and the number of systolic peaks (NSP) based PR estimation methods provide promising results for both normal and abnormal PPG signals.

3) PR ESTIMATION ANALYSIS USING BLAND-ALTMAN STATISTICS

In the past parameter estimation methods, the Bland-Altman plot analysis is performed for estimating a level of agreement between the actual and estimated PR values [55]. From the Bland-Altman plot, the following statistics such as bias, standard deviation (SD), limits of agreement (LOA), and Bland-Altman ratio (BAR) are computed for performance evaluation and comparison with other methods. For the signal durations of 10 and 60 seconds, Bland-Altman plots for four PR estimation methods are shown in Fig. 14 with LOA = Bias ± 1.96 SD. For the signal durations of 10, 20, 30, and 60 seconds, Bland-Altman plots are shown in Fig. 15 for the PE-based PR estimation methods. From the results, it is noticed that the FFT- based PR estimation method had a bias of 4.04 bpm with 95% agreement limits of [−8.46, 16.53] bpm whereas the ACF-based PR estimation method had a bias of 0.76 with 95% agreement limits of [7.22, −5.69] bpm. From the results as shown in Fig. 15, it is noticed that DPCM-based PR estimation method had a bias of 1.51 with 95% agreement limits of [−1.19, 3.20] bpm whereas from the results as shown in Fig. 14, it is noticed that the ATh-based method had the bias of −1.50 with 95% agreement limits of [−4.33, 1.32] bpm. Based on the overall estimation results of the bias, LOA, and BAR values, it is noted that the PE-based method had a higher degree of agreement between actual and estimated

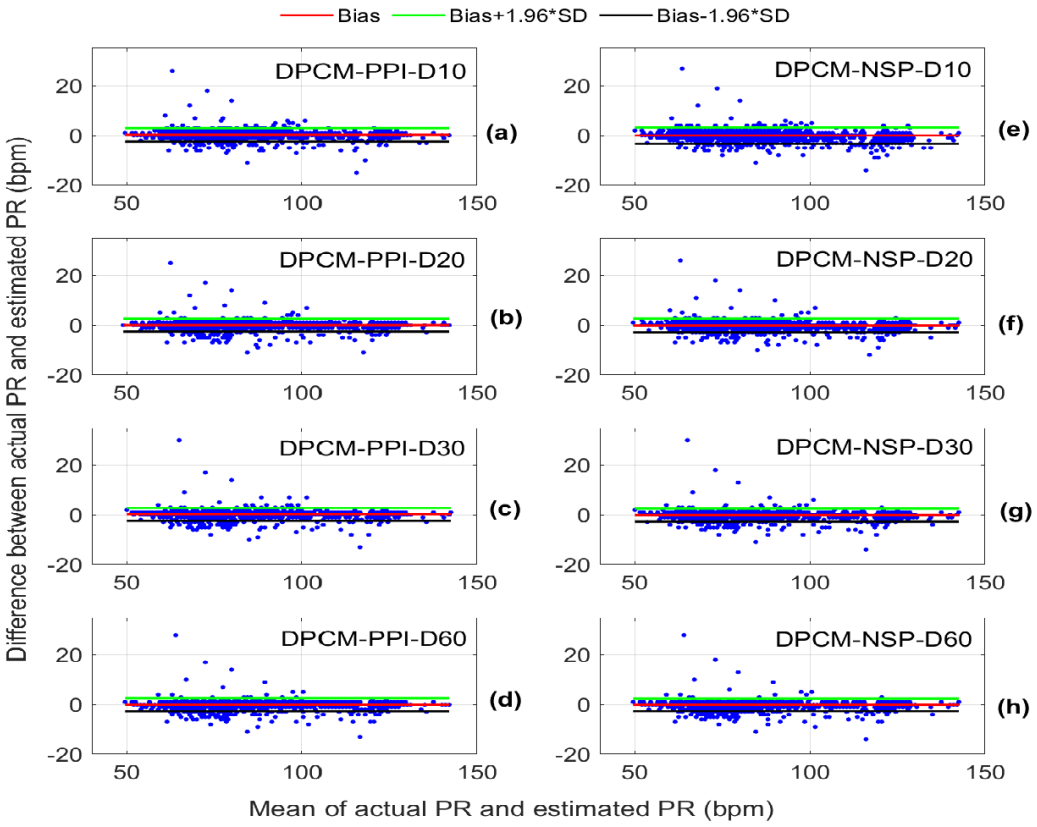

FIGURE 15. Bland-Altman plots of differences in actual and estimated PR measurements with the bias (red line) and 95% upper (green line) and lower (black line) limit of agreement (LOA) with Bias ± 1.96*SD, where SD is the standard deviation for PPI method (a)-(d) and NSP method (e-h) of duration 10, 20, 30, 60 seconds.

pulse rate values and thus outperforms other PR estimation methods.

4) COMPUTATIONAL COMPLEXITY OF PR ESTIMATION METHOD

In this paper, computational complexity analysis is performed in terms of the number of multiplications, additions, comparisons, and logical operations that are essential to demonstrate the real-time feasibility of the resource-constrained computing platform. For the PPG signals with sampling rates of 125 Hz and 25 Hz, computational loads (in terms of operations) and processing time (PT) are summarized in Table 6. In order to get the PR in beats per minute, for short PPG segments with durations of 10 and 30 seconds, the PR estimation method is executed 06 times and 02 times, respectively. From the results of the computational load, it is observed that the total number of operations of the PE- and ATh-based PR estimation methods is much lower than that of the FFT- and ACF-based methods for both sampling rates. Furthermore, for all signal durations with the sampling rates of 125 Hz and 25 Hz, the PE-based and ATh-based PR estimation methods outperform other methods in terms of estimation accuracy (resulting lesser number of segments with estimation error >5 bpm) and computational complexity. The ACF- and FFT-based PR estimation methods demand computational resources including memory space and energy consumption.

5) COMPARISON WITH OTHER PR ESTIMATION METHODS

In this study, we compare the performance of the proposed PR estimation method with the seven methods in terms of different performance metrics. Existing methods used different signal durations for estimating PR from the PPG signal and also different performance metrics for performance evaluation. In order to compare with all the methods, we evaluated the proposed method with signal durations of 10, 20, 30, and 60 seconds in terms of performance metrics such as mean absolute error (MAE), Pearson correlation coefficient (PCC), Bland-Altman ratio (BAR), root-mean-square error (RMSE) and average absolute error (AE). The evaluation results of this study are summarized in Table 7. Results demonstrate that the PE-based PR estimation method had a mean absolute error (MAE) of 0.46, Pearson correlation coefficient (PCC) of 0.9972, Bland-Altman ratio (BAR) of 3.04, and root-mean-square error (RMSE) of 1.28 for the PPG

TABLE 6. Computation complexity: Number of operations [multiplication (N_M), addition (N_A), comparison (N_C) and logical (N_L)] and N denotes the number of samples.

Duration (sec)	Method	PPG with Fs=125 Hz						PPG with Fs=25 Hz					
		N	N_M (k)	N_A (k)	N_C (k)	N_L (k)	PT (msec)	N	N_M (k)	N_A (k)	N_C	N_L	PT (msec)
10	FFT	2048	270.34	405.50	0.49	_	3.80	256	24.58	36.86	306	__	2.77
	ACF	1250	9375	9367.50	3	1.50	8.40	250	375	373.50	600	300	6.60
	PE	1250	37.49	104.91	29.98	7.49	156.00	250	7.49	5.97	5976	1494	41.40
	ATh	1250	7.50	_	52.49	15	11	250	1.5	_	10494	3000	10
30	FFT	4096	196.61	294.91	0.33	_	1.52	1024	40.96	61.44	408	__	1.42
	ACF	3750	28125	28117.5	1	0.50	4.00	750	1125	1123.50	200	100	2.40
	PE	3750	37.50	104.97	29.99	7.50	272.00	750	7.50	5.99	5992	1498	31.20
	ATh	3750	7.50	_	52.50	15	6	750	1.5	_	10498	3000	4
60	FFT	8192	212.99	319.49	0.33	_	1.00	2048	45.06	67.58	409	__	0.60
	ACF	7500	56250	56242.5	0.5	0.25	2.40	1500	2250	2248.50	100	50	1.40
	PE	7500	37.50	104.99	30.00	7.50	444.30	1500	7.50	5.995	5996	1499	33.50
	ATh	7500	7.50	_	52.50	15	4	1500	1.5	_	10499	3000	3

TABLE 7. Performance comparison of PR estimation methods.

Reference	Method	Dur. (sec)	Fs (Hz)	MAE ($\mu \pm \sigma$)	PCC	BAR (%)	RMSE	AE (%) ($\mu \pm \sigma$)	% of segments within ranges		
									PR $\pm$ 5 Error bpm (%)	PR $\pm$10 Error bpm (%)	$\lvert PR\rvert > 10$ Error bpm (%)
Garde [37]	EMD, PSD	60	100	NR	NR	NR	0.59	NR	NR	NR	NR
Saquib [60]	External BC,passive LPF,active HPF, Gain, NIB, PIC micro counter	15	NR	NR	NR	NR	NR	3.64%	NR	NR	NR
Gohlke [63]	PSD, digital BPF, normalization	25	400	NR	NR	NR	NR	NR	62.2	68.9	2.2
Zaeni [64]	Digital filtering, ATPD	4	100	NR	NR	NR	NR	2.05%	NR	NR	NR
Our Method (PE)	PPI	10	125	0.74±1.19	0.9968	3.3	1.40	0.93±1.67	99.21	99.81	0.19
	NSP	10	125	0.96±1.34	0.9955	3.9	1.65	1.17±1.81	99.09	99.81	0.19
	PPI	20	125	0.64±1.18	0.9970	3.2	1.34	0.80±1.64	99.05	99.81	0.19
	NSP	20	125	0.69±1.24	0.9966	3.4	1.42	0.84±1.70	98.96	99.84	0.16
	PPI	30	125	0.69±1.16	0.9970	3.2	1.35	0.86±1.68	99.31	99.87	0.13
	NSP	30	125	0.59±1.21	0.9969	3.2	1.35	0.73±1.72	99.24	99.84	0.16
	PPI	60	125	0.59±1.19	0.9970	3.2	1.33	0.73±1.68	99.09	99.84	0.16
	NSP	60	125	0.46±1.20	0.9972	3.0	1.28	0.57±1.68	99.15	99.84	0.16
Jaafar [65]	WD ,PSD	NR	NR	NR	NR	NR	NR	2.1-5.7	NR	NR	NR
Johnson [66]	LPF, TPD method	60	1000	9.20±6.42	NR	NR	NR	12.03±8.03	NR	NR	NR
Bagha [67]	LPF,MAF,APD.vi in LabView software	60	NR	1.50±2.51	NR	NR	NR	1.65±2.76	NR	NR	NR

Fs: Sampling frequency; AE: Absolute error; PCC: Pearson correlation coefficient; BAR: Bland-Altman ratio; PR= Pulse rate; PSD: Power spectral density; BPF: Band pass filter; EMD: Empirical mode decomposition; ATPD: Adaptive threshold peak detection; BC: Bias circuit; LPF: Low pass filter; HPF: High pass filter; NIB: Non inverting buffer; $\mathrm{PPI}_{\mathrm{avg}}$: Average Peak to Peak Interval; NSP: Number of systolic peaks; WD: Wavelet decomposition; TPD: Threshold based peak detection; MAF: Moving average filter,APD: Advanced peak detector, NR= Not reported.

Note: The result of [38], [62], [65], [66], [67], [68], [69] were taken from the corresponding references. The databases used in these references are created by corresponding authors and also those databases are not publicly available.

signal with a duration of 60 seconds. From the estimation results, it can be observed that the PE-based PR estimation method outperforms other PR estimation methods in terms of different kinds of performance metrics as reported in Table 7 with the use of simple prediction error-based onset and systolic peak detection method. The RMSE of the PE-based method is comparable with the RMSE of the EMD-based method [37]. Most existing methods used frequency-selective filters at the preprocessing stage to suppress the dominant low-frequency components and then used power spectral density (PSD) for determining pulse rate frequency from the processed signal. Some of the PR estimation methods used signal decomposition techniques such as empirical mode decomposition (EMD) and wavelet transform for selecting suitable PPG signal components and suppressing unwanted components. These methods demand more computational resources which are constrained with most wearable devices. Furthermore, it is observed that most methods use short

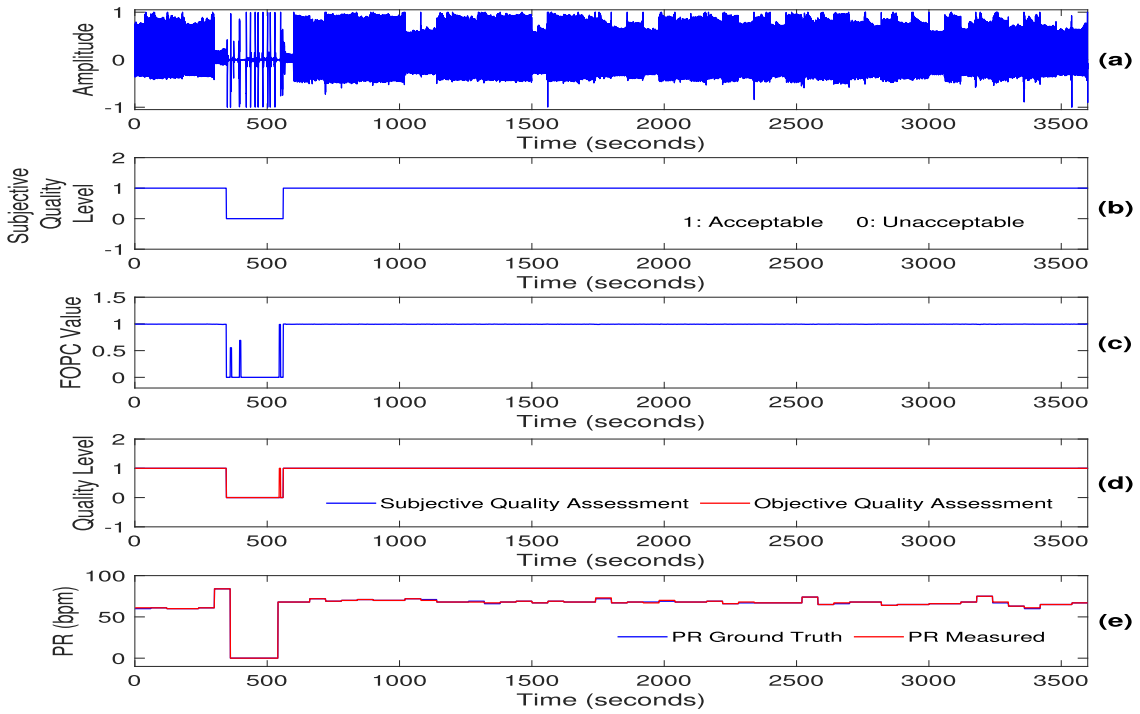

FIGURE 16. Results of quality-aware PR estimation (Record:slp01bm). (a) Original PPG signal, (b) subjective quality checking result (0 denotes bad quality and 1 denotes acceptable quality), quality rating using the first order predictor coefficient (FOPC) with on-width and off-width features, (d) combined results of subjective and objective checking and (e) Estimated PR with reference PR values.

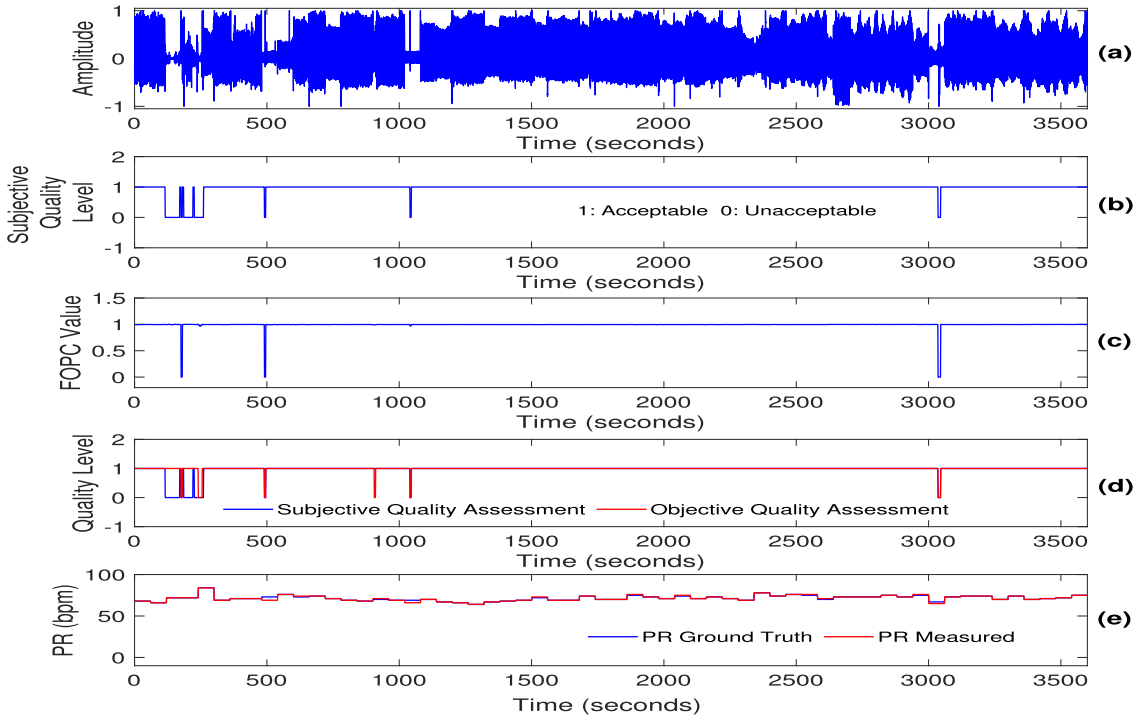

FIGURE 17. Results of quality-aware PR estimation (Record:slp41m).(a) Original PPG signal, (b) subjective quality checking result (0 denotes bad quality and 1 denotes acceptable quality), quality rating using the first order predictor coefficient (FOPC) with on-width and off-width features, (d) combined results of subjective and objective checking and (e) Estimated PR with reference PR values.

duration to estimate PR in beats per minute (bpm) which may not be accurate in practice when the PPG signals have varying pulse rates [23].

6) QUALITY-AWARE PR ESTIMATION RESULTS

One of the main objectives of this paper is to present quality-aware parameter estimation by exploring lightweight signal quality assessment methods. In this study, predictor coefficient and on-width and off-width duration features based on signal quality checking are incorporated before extracting the PR from the PPG signal. Subjective quality evaluation (SQE) assessment can evaluate the denoised or decompressed signal. In the SQE assessment test, biomedical experts visually inspect the preservation of important local waves and their fiducial points in the processed signal compared to the original signal and give a quality score on a 5-point scale (Excellent, Very Good, Good, Bad, and Very Bad), 3-point scale (Very Good, Good, and Bad), or 2-point scale (Acceptable or Unacceptable). Although the SQE assessment test can be used as the final score to judge the quality of the processed signal, it was observed that SQE tests are highly time-consuming and expensive, require experts' subject knowledge and cognitive skills, and cannot be incorporated with quality-control compression or denoising methods. Hence, objective quality assessment has become the main goal of many researchers to quantify waveform distortion to match expert's subjective evaluation score [56], [57]. Evaluation results of the proposed quality-aware parameter estimation method are shown in Figs. 16 and 17 for the recordings with noise-free PPG portions and noisy PPG portions. In the figures, the waveform in (a) denotes the original PPG signal with artifacts. the waveform in (b) denotes the result of quality checking via visual inspection (0 denotes unacceptable quality and 1 denotes acceptable quality), the waveform in (c) denotes the signal quality rating obtained by using the first order predictor coefficient (FOPC), the waveform in (d) denotes the final result of SQA based on the proposed number of threshold crossing (NTC), amplitude, FOPC, and on-width and off-width features as described in the Section III-A and subjective quality checking result, and waveform in (e) denotes the estimated PR and reference PR values by using the proposed quality-aware PR estimation method as described in the Section III-D. Results demonstrate the potentiality of the proposed quality-aware PR estimation in discarding the noisy PPG signals and reducing the false alarms due to the noisy measurements. Further, the quality-aware parameter estimation can reduce the overall energy consumption by discarding noisy PPG signal portions from the parameter extraction, data compression, and transmission stages of the on-device or edge health monitoring devices. Furthermore, quality checking can ensure the reliability of the vital sign estimation system under different recording conditions and also in the presence of various kinds of noises and artifacts, which are unavoidable under ambulatory and exercise PPG recording scenarios.

E. PERFORMANCE EVALUATION OF RR ESTIMATION METHODS

In this study, standard PPG signals that are taken from the CapnoBase datasets (http://www.capnobase.org/) and BIDMC database (https://archive.physionet.org/cgi-bin/atm/ATM) used for evaluating the performance of the respiratory-induced amplitude variation (RIAV), respiratory-induced intensity variation (RIIV), respiratory-induced frequency variation (RIFV) based RR estimation methods that are widely used in the past studies. The RR estimation performance is evaluated in terms of benchmark metrics such as the number of segments within the estimation error (EE) range (breaths per minute, (brpm)), mean absolute error (MAE) for each RR ranges, and MAE in terms of the median (25th-75th percentile). In this work, four respiration methods such as the RIAV, RIIV, and two RIFV based on the pulse-to-pulse (PPI) interval and foot-to-foot interval (FFI) are evaluated for the PPG signals with durations of 30 and 60 seconds. The estimation error ranges of 0, 1, 2, 3-4, 5-6, 7-10, and >10 (in number of breaths per minute, (brpm)). Further, the mean absolute error (MAE) is computed for five groups of respiration rates (<8, 8-12, 12-16, 16-20, and 20-30 breaths per minute). The ground-truth annotations are used for estimating the error between the actual and estimated value. Evaluation of this study is summarized in Table 8 for the PPG signals taken from the BIDMC database and in Table 9 for the PPG signals taken from the Capnobase database.

1) PERFORMANCE OF RR ESTIMATION ON DIFFERENT DATABASES

From evaluation results, it is observed that the respiration estimation method provides better results for PPG signals with a duration of 60 seconds as compared to the PPG signals with a duration of 30 seconds for both datasets. Results further show that the respiratory-induced intensity variation (RIIV) based RR estimation method had the mean absolute error (MAE) of 3.64 for 60 second PPG signal and MAE of 3.95 for 30 second PPG signal taken from the BIDMC database whereas RIIV based estimation method had the MAE of 3.08 for 60 second PPG signal and MAE of 3.51 for 30 second PPG signal taken from the Capnobase database. It is further observed that the RIIV-based estimation method outperforms the other three methods in terms of both average MAE and group-wise MAE and also the number of segments with an estimation error (EE) range. Fig. 18 shows the correlation between the reference RR and estimated RR for the PPG signals with durations of 30 and 60 seconds.

2) RR ESTIMATION COMPARISON WITH EXISTING METHODS

In this study, the performance of the prediction error (PE) based RR estimation method is compared with existing methods which are tested with BIDMC and Capnobase databases. The evaluation results of this study are summarized in Table 10. The PE-RIIV based RR estimation method

TABLE 8. Performance of RR estimation methods on BIDMC database.

Dur. (sec)	Method	BIDMC database												
		Number of Segments within EE Range (breaths per minute, (brpm))								MAE				
		0	1	2	3-4	5-6	7-10	>10	MAE	<8	8-12	12-16	16-20	20-30
60	RIAV_FFT	107	98	13	27	23	70	86	4.80	3.88	2.06	3.87	4.90	6.45
	RIIV_FFT	153	121	14	11	12	50	63	3.64	0.75	1.94	2.56	3.55	5.65
	RIFV_PPI_FFT	78	72	18	26	16	78	136	6.82	1.50	6.56	7.15	6.48	7.01
	RIFV_FFI_FFT	76	82	20	31	26	78	111	6.22	9.00	5.63	6.21	6.02	6.44
30	RIAV_FFT	134	193	59	54	51	148	209	5.80	5.11	4.16	4.81	5.73	7.82
	RIIV_FFT	192	286	65	44	39	99	123	3.95	1.78	2.24	2.80	4.01	5.99
	RIFV_PPI_FFT	109	136	53	49	54	133	314	7.75	9.44	8.05	7.87	7.17	8.14
	RIFV_FFI_FFT	111	133	69	52	51	135	297	7.36	11.50	6.58	7.26	7.28	7.63

TABLE 9. Performance of RR estimation methods on Capnobase datasets.

Dur. (sec)	Method	Capnobase													
		Number of Segments within EE Range (brpm)								MAE					
		0	1	2	3-4	5-6	7-10	>10	MAE	<8	8-12	12-16	16-20	20-30	30-40	40-60
60	RIAV_FFT	113	114	11	17	19	23	39	3.50	5.00	3.36	2.34	2.00	2.37	12.81	14.60
	RIIV_FFT	115	136	7	16	8	22	32	3.08	3.50	2.26	1.67	1.64	5.11	16.06	7.00
	RIFV_PPI_FFT	120	103	11	29	19	17	37	3.28	1.10	2.94	1.88	2.07	5.63	9.19	12.00
	RIFV_FFI_FFT	124	95	13	29	16	19	40	3.56	6.60	2.77	1.47	7.21	3.24	8.06	10.20
30	RIAV_FFT	69	248	110	47	56	53	89	4.24	5.41	4.00	3.98	2.61	3.29	11.78	9.33
	RIIV_FFT	90	272	143	24	27	54	62	3.51	3.48	2.96	2.68	1.99	4.68	13.50	6.00
	RIFV_PPI_FFT	92	238	90	71	51	47	83	4.46	2.41	4.13	2.69	1.73	7.83	13.17	6.42
	RIFV_FFI_FFT	74	233	99	66	43	55	102	4.97	5.74	4.41	2.92	7.19	5.32	12.42	1.08

TABLE 10. Performance comparison of RR estimation methods.

Reference	Method	MAE in terms of median (25th-75th percentiles)			
		Duration=30 seconds		Duration=60 seconds	
		BIDMC	CapnoBase	BIDMC	CapnoBase
Our Method	RIAV_FFT	5.2(4.1-7.9)	4.0(1.6-6.1)	4.4(2.5-7.0)	2.4(0.8-5.0)
	RIIV_FFT	3.1(1.5-5.6)	2.4(1.4-3.9)	2.5(0.8-4.9)	1.0(0.5-4.0)
	RIFV_PPI_FFT	8.0(5.5-9.8)	2.8(1.3-5.3)	6.6(4.2-9.5)	2.3(0.6-4.3)
	RIFV_FFI_FFT	7.3(4.8-9.9)	3.7(1.6-6.3)	5.6(3.8-9.1)	2.2(0.5-4.6)
Karlen [45]	IMSA, RIIV, RIFV, RIAV, FFT, SF method	5.8 (1.9-9.7)	1.2 (0.5-3.4)	5.7 (1.5-9.7)	0.8 (0.3-2.7)
Nilsson [46]	RIIV, BPF, visual inspection & BD algorithm	5.4 (3.4-9.2)	10.5(4.9-12.7)	4.6(2.5-8.5)	10.2 (4.8-12.4)
Pimentel [10]	Multiple AR models of different orders in the RIIV, RIFV, RIAV	4 (1.8-5.5)	1.5(0.3-3.3)	2.7 (1.5-5.3)	1.9 (0.3-3.4)
Shelley [62]	PD algorithm , STFT, Hann window	3.5 (1.5-9.4)	4.5(0.8-10.5)	2.3(0.9-7.9)	2.2 (0.2-8.3)
Fleming [68]	AR model and downsampled	5.2 (2.6-7.7)	1.4(0.5-3.8)	5.5 (2.7-8.1)	1.1 (0.4-3.5)

IMSA: Incremental-Merge Segmentation algorithm; RIIV: Respiration induced intensity variation; RIAV: Respiration induced amplitude variation; RIFV: Respiration induced frequency variation; FFT: fast Fourier transforms, SF:Smart fusion; AR: Autoregressive; PD: Peak detection; STFT: Short time Fourier transform; BPF: Band pass filter; BD: Breath detection;
Note: The result of [45], [46], [10], [62], and [68] was reported by the author Pimentel in [10].

outperforms other existing methods for the BIDMC database for the PPG signals with durations of 30 and 60 seconds. It is further observed that the PE-RIIV based RR estimation method outperforms the RR estimation method reported in [62] based on the peak detection, short-time Fourier transform (STFT) and Hanning window, and estimation

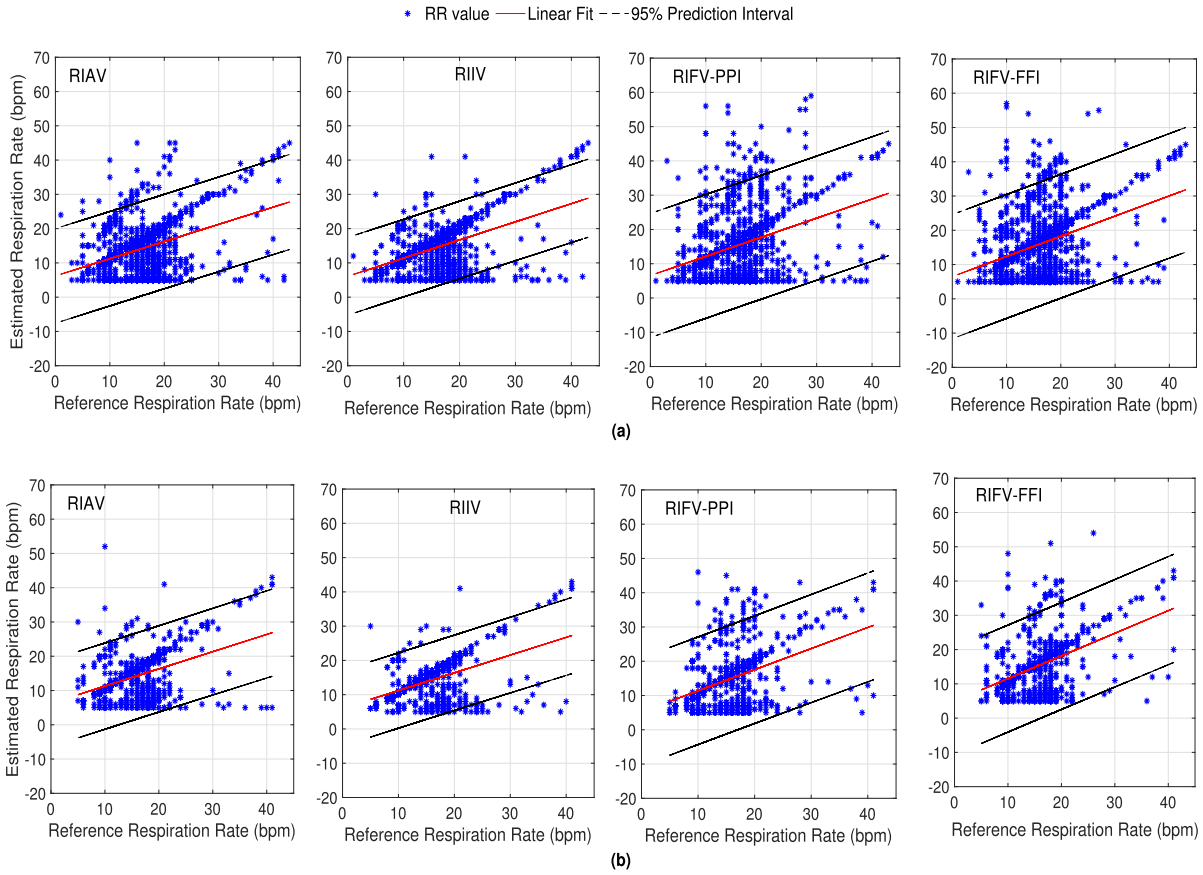

FIGURE 18. Scatter plot comparing the reference RR with the estimated RR from the PPG collected from the CapnoBase and BIDMC dataset using the proposed method for (a) 30 second (b) 60 second.

method reported in [46] based on the RIIV, bandpass filter, visual inspection and breath detection algorithms for the PPG signals taken from the Capnobase database. Although the estimation methods reported in Refs. [45] and [68] perform well as compared to other methods, the real-time implementation is not addressed which is most important for studying the real-time feasibility of the algorithms on the resource-constrained devices. Further, these methods used computationally expensive algorithms which may demand more computational resources for both storing and processing.

V. REAL-TIME IMPLEMENTATION AND ENERGY CONSUMPTION AND PROCESSING TIME ANALYSIS

A unified quality-aware PPG data compression and pulse- and respiration-rate estimation framework is proposed for energy-constrained wearable and edge PPG monitoring devices. The main objectives of this study are: to minimize the total energy consumption by exploring lightweight time-domain signal processing techniques which can be suitable for performing joint data compression, signal quality assessment, and PR-RR parameter extraction without the use of different domains of signal processing techniques; and to enable quality-aware wireless data transmission and also quality-aware parameter extraction which can significantly reduce energy consumption and false alarm rate, respectively by discarding the severely corrupted PPG signals.

1) REAL-TIME IMPLEMENTATION OF QUALITY-AWARE PROPOSED FRAMEWORK

In this study, real-time implementation of a unified quality-aware compression and pulse-respiration rates estimation framework is performed by using the Arduino Due computing platform with specifications of Atmel SAM3X8E ARM Cortex-M3 processor with 512-kB flash memory, 96-kB SRAM, and 84-MHz clock speed, the Bluetooth low energy (BLE) and Smartphone as shown in Fig. 19. The Arduino Due is interfaced with pulse sensing and BLE modules. The BLE is used for wirelessly transmitting acceptable quality PPG signals to smartphones, which can be used as the ‘‘base station’’ in wearable body area networks.

2) PERFORMANCE METRICS AND ENERGY SAVING ANALYSIS

The performance of the proposed unified framework is evaluated in terms of computational time and energy

consumption by using noise-free and noisy normal and abnormal PPG signals. The significance of the unified framework is assessed in terms of false alarm reduction rate (FARR), sensitivity (Se), compression ratio (CR) with percent root mean square difference (PRD), PR and RR measurement accuracy, memory size, and percentage of energy saving. In order to have a meaningful comparison, the energy consumption analysis of existing PR-RR estimation methods is performed by using the PPG signals which are digitized with sampling rates of 125 Hz and 25 Hz because these two sampling rates are widely used in past studies. For the PPG signals with a duration of 60 s and 30 s, Table 11 summarizes energy consumption for each stage of unified predictive coding based on quality-aware data compression and PR-RR estimation framework and uncompressed methods. The processing stages are: pre-processing, signal quality assessment (SQA), compression, PR estimation, RR estimation, and data transmission. All these stages are implemented in real-time using the Arduino Due computing platform. In this study, uncompressed PPG signals sampled at the rates of 125 Hz and 25 Hz are used for extracting pulse rate and respiration rate directly from the PPG signal with quality checking and then transmitted directly to the Smartphone without compression of the PPG signal. From the performance evaluation results, it can be observed that the total computational time for the processing of the PPG signals with a sampling rate of 25 Hz is lesser than the computational times of the PPG signal with a sampling rate of 125 Hz and predictive coding-based unified framework. However, the total computational time for the predictive coding-based unified framework is lesser than the computational time of the PPG signal with a sampling rate of 125 Hz and also comparable with that of the processing time of the PPG signal with a sampling rate of 25 Hz.

Fig. 20 demonstrates the real-time implementation of unified predictive coding based quality-aware data compression and PR-RR estimation framework with estimated parameters such as signal quality assessment, compression ratio (CR), pulse rate (PR), and respiration rate (RR). For on-device vital sign monitoring, the proposed quality-aware framework is faster in measuring pulse rate and respiration rate in the compressed domain as compared to the original PPG signal with a sampling rate of 125 Hz. However, the effectiveness of the framework must be evaluated in terms of energy consumption because the processing times for all three frameworks are within the duration of the processed PPG signal. From the energy consumption results as reported in Table 11, it can be observed that the predictive coding-based quality-aware framework had an energy saving of 70.28% as compared to the uncompressed framework with a sampling rate of 125 Hz meanwhile it needs extra energy as compared to the uncompressed framework with a sampling rate of 25 Hz. Although the energy saving to maximize life-time of the battery is an important, accurate, and reliable measurement of pulse rate and respiration rate is essential

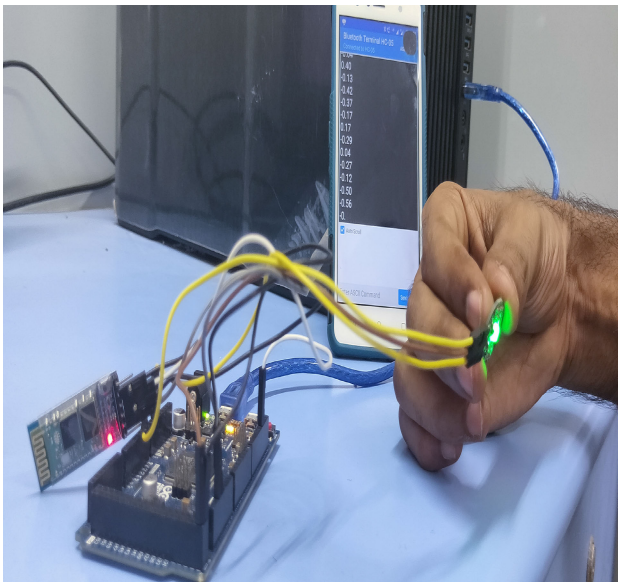

FIGURE 19. Real-time data transmission after data compressed data and quality checking from Arduino Due computing platform to Smartphone using Bluetooth module and Pulse sensor have a green LED from Kingbright (AM2520ZGC09) with a peak wavelength of 515 nm, and Photo sensor from Avago (APDS-9008) with a peak sensitivity at 565 nm.

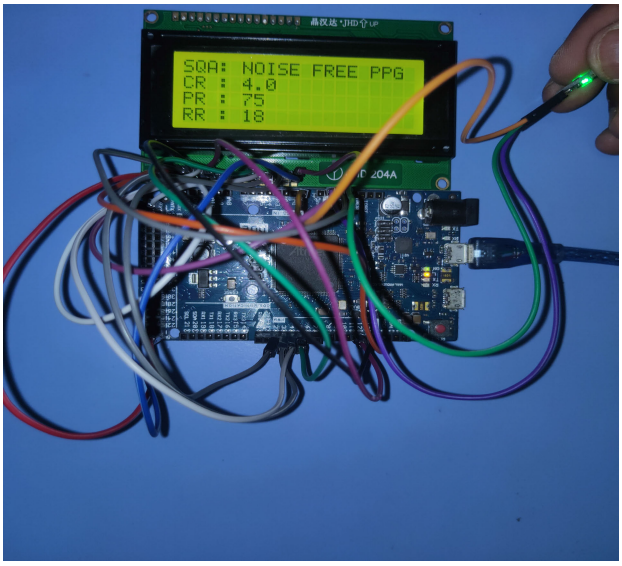

FIGURE 20. Real-time implementation of unified predictive coding based quality-aware data compression and PR-RR estimation framework with estimated parameters such as signal quality assessment, compression ratio (CR), pulse rate (PR), and respiration rate (RR).

for accurate diagnosis of different kinds of PPG-derived diseases. Therefore, the final comparison of three frameworks (proposed predictive coding (PC) based framework, 125 Hz sampling rate based framework, and 25 Hz sampling rate based framework) is reported in Table 11 in terms of sensitivity (Se), false alarm reduction rate (FARR), PR and RR estimation accuracies in addition to the processing time, energy consumption and memory space. The unified predictive coding-based quality-aware framework had better

TABLE 11. Performance comparison of proposed unified frameworks for the duration of 60 and 30 seconds, in terms of false alarm reduction rate (FARR), sensitivity (Se), compression ratio (CR) with percent root mean square difference (PRD), PR and RR measurement accuracy, memory size and percentage of energy saving.

Signal Duration, D=60 seconds											
Method	SQA		PR	RR	CR	PRD	Total Time (sec)	Total Memory (KB)	Total EC (mJ)	Energy Saving w.r.t. Fs=125 Hz	Energy Saving w.r.t. Fs=25 Hz
	Se (%)	FARR (%)	(MAE±SD)	MAE Median (25-75)							
Fs=125 Hz	90.70	84.65	0.43±1.45	1.75 (0.95-4.25)	NA	NA	52.40±0.034	149.43	9587.44±0.011	NA	NA
Fs=25 Hz	90.70	84.65	0.53±1.28	1.85(0.9-4.2)	5	1.26±0.65	10.56±0.0045	71.12	1934.53±0.001	79.83% saving	NA
PC with Fs=125 Hz	92.00	84.87	0.46±1.20	1.75(0.65-4.45)	4	3.22±1.91	15.34±0.010	337.29	2849.93±0.001	70.28% saving	32.12% extra
Signal Duration, D=30 seconds											
Method	SQA		PR	RR	CR	PRD	Total Time (sec)	Total Memory (KB)	Total EC (mJ)	Energy Saving w.r.t. Fs=125 Hz	Energy Saving w.r.t. Fs=25 Hz
	Se (%)	FARR (%)	(MAE±SD)	MAE Median (25-75)							
Fs=125 Hz	90.70	84.65	0.50±1.47	3.2(1.75-5.65)	NA	NA	26.20±0.022	74.72	4793.84±0.010	NA	NA
Fs=25 Hz	90.70	84.65	0.70±1.33	3.4(1.8-5.95)	5	1.26±0.65	5.28±0.077	35.56	967.47±0.001	79.81% saving	NA
PC with Fs=125 Hz	92.00	84.87	0.59±1.21	2.75(1.45-4.75)	4	3.22±1.91	7.66±0.0051	168.65	1423.16±0.001	70.31% saving	32.04% extra

signal quality assessment accuracy and PR and RR estimation accuracies as compared to the other two frameworks with the uncompressed PPG signals (125 Hz and 25 Hz sampling rate). Moreover, a high-resolution PPG signals with a higher sampling rate (for example, 125 Hz) is most important for accurately determining the fiducial points (onset, maximum slope point, tidal peak, dicrotic notch, diastolic peak) of the PPG signal and then estimating other PPG parameters such as pulse width, pulse area, crest-time, decay-time, inflection point area, atrial stiffness and so on for automatic diagnosis of cardiovascular diseases. In the PPG waveform delineation process, due to the error of one sample (a sampling interval, $T_s = \frac{1}{F_s}$), the minimum fiducial time instant estimation error for the uncompressed PPG signal is 8 ms for a sampling rate of 125 Hz and is 50 ms for a sampling rate of 25 Hz. In this study, we noticed that the PPI estimation error is higher for the case of PPG signal with a sampling rate of 25 Hz as compared to that of the uncompressed PPG with a sampling rate of 125 Hz and also the proposed prediction error based PPI estimation method that can be seen in the PR estimation results as summarized in Table 4 and Table 5. Thus, an uncompressed PPG signal with a sampling rate of 25 Hz would have a larger estimation error in the measurement of the above-mentioned PPG parameters as compared to the PPG signal with a sampling rate of 125 Hz.

VI. CONCLUSION

Due to the device's miniaturization with tiny battery size and the presence of unavoidable movement artifacts and other noise sources, improvement of energy efficiency and false alarm reduction rate (FARR) has become essential for maximizing battery life-time and reducing false alarms leading to the long-term vital sign sensing and improving the accuracy and reliability of wearable or portable PPG-based health status monitoring and drug delivery devices. By considering the resource constraints, this paper presented the unified quality-aware data compression and pulse-respiration rates estimation framework by exploring lightweight signal processing techniques such as the predictive coding and time-domain waveform features for performing the following PPG processing tasks such as signal quality assessment, data compression, onset-peak detection, pulse rate, and respiration rate estimation by processing the intermediate waveforms of the predictive coding. The proposed framework is tested by using a wide variety of PPG signals taken from five standard databases and its real-time implementation is performed by using the Arduino Due computing platform with specifications of ARM Cortex-M3 processor with 512-kB flash memory, 96-kB SRAM, and 84-MHz clock speed interfaced with Smartphone using the Bluetooth low energy (BLE) module. Performance of each of the processing tasks of the unified framework was evaluated in terms of sensitivity (Se) and FARR for the SQA method, compression ratio (CR) and PRD for the data compression, mean absolute error (MAE) for the PR and RR estimation and energy consumption and processing time for the overall performance of the unified framework. As compared with the performance of uncompressed PPG signal-based framework with a sampling rate of 125 Hz, the proposed unified framework outperforms in terms of Se and FARR of the SQA, accuracies of PR and RR estimation, processing time, and energy consumption. The proposed predictive coding-based quality-aware PPG processing framework had an energy saving of 70.28% as compared to the uncompressed framework with a sampling rate of 125 Hz. Evaluation results demonstrated that the proposed unified quality-aware PR-RR estimation, data compression, and transmission framework has great potential to improve energy efficiency (maximizing battery life) of the energy-constrained device, and improving

the trustworthiness of health monitoring devices by reducing false alarms by using the signal quality checking methodology. Arduino Due computing platform-based implementation demonstrates the real-time feasibility of the proposed unified quality-aware PPG processing framework on the limited computational resources.

ACKNOWLEDGMENT

The author Sabarimalai Manikandan was with the Indian Institute of Technology Bhubaneswar, Odisha.

REFERENCES

[1] U. Satija, B. Ramkumar, and M. S. Manikandan, "Real-time signal quality-aware ECG telemetry system for IoT-based health care monitoring," *IEEE Internet Things J.*, vol. 4, no. 3, pp. 815–823, Jun. 2017.

[2] S. Vadrevu and M. S. Manikandan, "Real-time quality-aware PPG waveform delineation and parameter extraction for effective unsupervised and IoT health monitoring systems," *IEEE Sensors J.*, vol. 19, no. 17, pp. 7613–7623, Sep. 2019.

[3] S. Vadrevu and M. S. Manikandan, "A new quality-aware quality-control data compression framework for power reduction in IoT and smartphone PPG monitoring devices," *IEEE Sensors Lett.*, vol. 3, no. 7, pp. 1–4, Jul. 2019.

[4] K. Manojkumar, S. Boppu, and M. S. Manikandan, "An automated algorithm for estimating respiration rate from PPG signals," in *Proc. Int. Conf. Mach. Learn. Image Process. Netw. Secur. Data Sci. (MIND)*, vol. 1241, 2020, pp. 44–57.

[5] M. Chan, V. G. Ganti, and O. T. Inan, "Respiratory rate estimation using U-Net-based cascaded framework from electrocardiogram and seismocardiogram signals," *IEEE J. Biomed. Health Informat.*, vol. 26, no. 6, pp. 2481–2492, Jun. 2022.

[6] S. Lee, H. Moon, C.-H. Son, and G. Lee, "Respiratory rate estimation combining autocorrelation function-based power spectral feature extraction with gradient boosting algorithm," *Appl. Sci.*, vol. 12, no. 16, p. 8355, Aug. 2022.

[7] B. Roy, A. Roy, J. K. Chandra, and R. Gupta, "I-PRExT: Photoplethysmography derived respiration signal extraction and respiratory rate tracking using neural networks," *IEEE Trans. Instrum. Meas.*, vol. 70, 2021, Art. no. 2504309.

[8] T. Iqbal, A. Elahi, S. Ganly, W. Wijns, and A. Shahzad, "Photoplethysmography-based respiratory rate estimation algorithm for health monitoring applications," *J. Med. Biol. Eng.*, vol. 42, no. 2, pp. 242–252, Apr. 2022.

[9] S. Ismail, I. Siddiqi, and U. Akram, "Heart rate estimation in PPG signals using convolutional-recurrent regressor," *Comput. Biol. Med.*, vol. 145, Jun. 2022, Art. no. 105470.

[10] M. A. F. Pimentel, A. E. W. Johnson, P. H. Charlton, D. Birrenkott, P. J. Watkinson, L. Tarassenko, and D. A. Clifton, "Toward a robust estimation of respiratory rate from pulse oximeters," *IEEE Trans. Biomed. Eng.*, vol. 64, no. 8, pp. 1914–1923, Aug. 2017.

[11] Z. Cohen and S. Haxha, "Optical-based sensor prototype for continuous monitoring of the blood pressure," *IEEE Sensors J.*, vol. 17, no. 13, pp. 4258–4268, Jul. 2017.

[12] A. M. Nia, M. Mozaffari-Kermani, S. Sur-Kolay, A. Raghunathan, and N. K. Jha, "Energy-efficient long-term continuous personal health monitoring," *IEEE Trans. Multi-Scale Comput. Syst.*, vol. 1, no. 2, pp. 85–98, Apr. 2015.

[13] W. Zuo, P. Wang, and D. Zhang, "Comparison of three different types of wrist pulse signals by their physical meanings and diagnosis performance," *IEEE J. Biomed. Health Informat.*, vol. 20, no. 1, pp. 119–127, Jan. 2016.

[14] G. N. K. Reddy, M. S. Manikandan, and N. V. L. N. Murty, "On-device integrated PPG quality assessment and sensor disconnection/saturation detection system for IoT health monitoring," *IEEE Trans. Instrum. Meas.*, vol. 69, no. 9, pp. 6351–6361, Sep. 2020.

[15] U. Satija, B. Ramkumar, and M. S. Manikandan, "A review of signal processing techniques for electrocardiogram signal quality assessment," *IEEE Rev. Biomed. Eng.*, vol. 11, pp. 36–52, 2018.

[16] U. Satija, B. Ramkumar, and M. S. Manikandan, "A new automated signal quality-aware ECG beat classification method for unsupervised ECG diagnosis environments," *IEEE Sensors J.*, vol. 19, no. 1, pp. 277–286, Jan. 2019.

[17] K. Li, S. Warren, and B. Natarajan, "Onboard tagging for real-time quality assessment of photoplethysmograms acquired by a wireless reflectance pulse oximeter," *IEEE Trans. Biomed. Circuits Syst.*, vol. 6, no. 1, pp. 54–63, Feb. 2012.

[18] C. Fischer, B. Dömer, T. Wibmer, and T. Penzel, "An algorithm for real-time pulse waveform segmentation and artifact detection in photoplethysmograms," *IEEE J. Biomed. Health Inform.*, vol. 21, no. 2, pp. 372–381, Mar. 2017.

[19] D. Dao, S. M. A. Salehizadeh, Y. Noh, J. W. Chong, C. H. Cho, D. McManus, C. E. Darling, Y. Mendelson, and K. H. Chon, "A robust motion artifact detection algorithm for accurate detection of heart rates from photoplethysmographic signals using time-frequency spectral features," *IEEE J. Biomed. Health Inform.*, vol. 21, no. 5, pp. 1242–1253, Sep. 2017.

[20] M. Hooshmand, D. Zordan, D. D. Testa, E. Grisan, and M. Rossi, "Boosting the battery life of wearables for health monitoring through the compression of biosignals," *IEEE Internet Things J.*, vol. 4, no. 5, pp. 1647–1662, Oct. 2017.

[21] S. Vadrevu and M. S. Manikandan, "Real-time PPG signal quality assessment system for improving battery life and false alarms," *IEEE Trans. Circuits Syst. II, Exp. Briefs*, vol. 66, no. 11, pp. 1910–1914, Nov. 2019.

[22] G. N. K. Reddy, M. S. Manikandan, and N. V. L. N. Murty, "Lightweight compressed sensing (CS) and partial DCT based compression schemes for energy-efficient wearable PPG monitoring devices," in *Proc. IEEE Int. Conf. Health, Instrum. Meas., Natural Sci. (InHeNce)*, Jul. 2021, pp. 1–6.

[23] G. N. K. Reddy, M. S. Manikandan, and N. V. L. N. Murty, "Performance of spectral, autocorrelation and peak count based PR estimation methods under normal/abnormal PPG for wearable devices," in *Proc. IEEE Int. Conf. Health, Instrum. Meas., Natural Sci. (InHeNce)*, Indonesia, Jul. 2021, pp. 14–16.

[24] C. Orphanidou, T. Bonnici, P. Charlton, D. Clifton, D. Vallance, and L. Tarassenko, "Signal-quality indices for the electrocardiogram and photoplethysmogram: Derivation and applications to wireless monitoring," *IEEE J. Biomed. Health Informat.*, vol. 19, no. 3, pp. 832–838, May 2015.

[25] Q. Li and G. D. Clifford, "Dynamic time warping and machine learning for signal quality assessment of pulsatile signals," *Physiol. Meas.*, vol. 33, no. 9, pp. 1491–1501, Sep. 2012.

[26] W. Karlen, J. M. Ansermino, and G. Dumont, "Adaptive pulse segmentation and artifact detection in photoplethysmography for mobile applications," in *Proc. Annu. Int. Conf. IEEE Eng. Med. Biol. Soc.*, Aug. 2012, pp. 3131–3134.

[27] E. Sabeti, N. Reamaroon, M. Mathis, J. Gryak, M. Sjoding, and K. Najarian, "Signal quality measure for pulsatile physiological signals using morphological features: Applications in reliability measure for pulse oximetry," *Informat. Med. Unlocked*, vol. 16, Jan. 2019, Art. no. 100222.

[28] G. N. K. Reddy, M. S. Manikandan, and N. V. L. N. Murty, "Integrated data compression and pulse rate extraction scheme using differential coding for wireless PPG monitoring devices," in *Proc. IEEE 13th Int. Conf. Ind. Inf. Syst. (ICIIS)*, Dec. 2018, pp. 48–53.

[29] J. Makhoul, "Linear prediction: A tutorial review," *Proc. IEEE*, vol. 63, no. 4, pp. 561–580, Apr. 1975.

[30] T. Tamura, Y. Maeda, M. Sekine, and M. Yoshida, "Wearable photoplethysmographic sensors—Past and present," *Electronics*, vol. 3, no. 2, pp. 282–302, Apr. 2014.

[31] D. S. Raju, M. S. Manikandan, and R. Barathram, "An automated method for detecting systolic peaks from arterial blood pressure signals," in *Proc. IEEE Students' Technol. Symp.*, Feb. 2014, pp. 41–46.

[32] S. Vadrevu and M. S. Manikandan, "Effective systolic peak detection algorithm using variational mode decomposition and center of gravity," in *Proc. IEEE Region Conf. (TENCON)*, Nov. 2016, pp. 2711–2715.

[33] S. Vadrevu and M. S. Manikandan, "A robust pulse onset and peak detection method for automated PPG signal analysis system," *IEEE Trans. Instrum. Meas.*, vol. 68, no. 3, pp. 807–817, Aug. 2019.

[34] G. N. K. Reddy, M. S. Manikandan, and N. V. L. N. Murty, "Predictive coding with simultaneous extraction of pulse and respiration rates from PPG signal for energy constrained wearable devices," in *Proc. 4th Int. Conf. Bio-Eng. Smart Technol. (BioSMART)*, Paris, France, Dec. 2021, pp. 8–10.

[35] E. D. Giovanni, S. Murali, F. Rincon, and D. Atienza, "Ultra-low power estimation of heart rate under physical activity using a wearable photoplethysmographic system," in *Proc. Euromicro Conf. Digit. Syst. Design (DSD)*, Aug. 2016, pp. 553–560.

[36] R. Aisuwarya, H. Hendrick, and M. Meitiza, "Analysis of cardiac frequency on photoplethysmograph (PPG) synthesis for detecting heart rate using fast Fourier transform (FFT)," in *Proc. Int. Conf. Electr. Eng. Comput. Sci. (ICECOS)*, Oct. 2019, pp. 391–395.

[37] A. Garde, W. Karlen, P. Dehkordi, J. M. Ansermino, and G. A. Dumont, "Empirical mode decomposition for respiratory and heart rate estimation from the photoplethysmogram," in *Proc. Comput. Cardiol.*, 2013, pp. 799–802.

[38] J. Allen, "Photoplethysmography and its application in clinical physiological measurement," *Physiol. Meas.*, vol. 28, no. 3, pp. R1–R39, Mar. 2007.

[39] V. Hartmann, H. Liu, F. Chen, W. Hong, S. Hughes, and D. Zheng, "Toward accurate extraction of respiratory frequency from the photoplethysmogram: Effect of measurement site," *Frontiers Physiol.*, vol. 10, p. 732, Jun. 2019.

[40] H. Liu, F. Chen, V. Hartmann, S. G. Khalid, S. Hughes, and D. Zheng, "Comparison of different modulations of photoplethysmography in extracting respiratory rate: From a physiological perspective," *Physiol. Meas.*, vol. 41, no. 9, Oct. 2020, Art. no. 094001.

[41] K. Nakajima, T. Tamura, T. Ohta, H. Miike, and P. A. Oberg, "Photoplethysmographic measurement of heart and respiratory rates using digital filters," in *Proc. 15th Annu. Int. Conf. IEEE Eng. Med. Biol. Societ*, Oct. 1993, pp. 1006–1007.

[42] L.-G. Lindberg, H. Ugnell, and P. Å. Öberg, "Monitoring of respiratory and heart rates using a fibre-optic sensor," *Med. Biol. Eng. Comput.*, vol. 30, no. 5, pp. 533–537, Sep. 1992.

[43] K. Nakajima, T. Tamura, and H. Miike, "Monitoring of heart and respiratory rates by photoplethysmography using a digital filtering technique," *Med. Eng. Phys.*, vol. 18, pp. 365–372, Jul. 1996.

[44] J. Li, J. Jin, X. Chen, W. Sun, and P. Guo, "Comparison of respiratory-induced variations in photoplethysmographic signals," *Physiol. Meas.*, vol. 31, no. 3, pp. 415–425, Mar. 2010.

[45] W. Karlen, S. Raman, J. M. Ansermino, and G. A. Dumont, "Multiparameter respiratory rate estimation from the photoplethysmogram," *IEEE Trans. Biomed. Eng.*, vol. 60, no. 7, pp. 1946–1953, Jul. 2013.

[46] L. Nilsson, A. Johansson, and S. Kalman, "Monitoring of respiratory rate in postoperative care using a new photoplethysmographic technique," *J. Clin. Monit. Comput.*, vol. 16, no. 4, pp. 309–315, May 2000.

[47] A. Johansson and P. Å. Öberg, "Estimation of respiratory volumes from the photoplethysmographic signal. Part I: Experimental results," *Med. Biol. Eng. Comput.*, vol. 37, no. 1, pp. 42–47, Jan. 1999.

[48] L. Nilsson, A. Johansson, J. Svanerudh, and S. Kalman, "Is the respiratory component of the photoplethysmographic signal of venous origin?" *Med. Biol. Eng. Comput.*, vol. 37, pp. 912–913, 1999.

[49] P. Dehkordi, A. Garde, B. Molavi, C. L. Petersen, J. M. Ansermino, and G. A. Dumont, "Estimating instantaneous respiratory rate from the photoplethysmogram," in *Proc. 37th Annu. Int. Conf. IEEE Eng. Med. Biol. Soc. (EMBC)*, Aug. 2015, pp. 6150–6153.

[50] H. Ugnell, "Photoplethysmographic heart and respiratory rate monitoring," M.S. thesis, Dept. Biomed. Eng., Linkping Univ., Linkping, Sweden, 1995.

[51] P. S. Addison, J. N. Watson, M. L. Mestek, and R. S. Mecca, "Developing an algorithm for pulse oximetry derived respiratory rate (RRoxi): A healthy volunteer study," *J. Clin. Monitor. Comput.*, vol. 26, no. 1, pp. 45–51, Feb. 2012.

[52] P. Dehkordi, A. Garde, B. Molavi, J. M. Ansermino, and G. A. Dumont, "Extracting instantaneous respiratory rate from multiple photoplethysmogram respiratory-induced variations," *Frontiers Physiol.*, vol. 9, p. 948, Jul. 2018.

[53] Complex System Laboratory. *CSL Benchmark Dataset*. Accessed: Apr. 4, 2018. [Online]. Available: http://bsp.pdx.edu/Data/

[54] *The MIT-BIH Polysomnographic Database*. Accessed: May 24, 2016. [Online]. Available: https://physionet.org/physiobank/database/slpdb/

[55] A. Bánhalmi, J. Borbás, M. Fidrich, V. Bilicki, Z. Gingl, and L. Rudas, "Analysis of a pulse rate variability measurement using a smartphone camera," *J. Healthcare Eng.*, vol. 2018, pp. 1–15, Feb. 2018.

[56] G. N. K. Reddy, M. S. Manikandan, and N. V. L. N. Murty, "Evaluation of objective distortion measures for automatic quality assessment of processed PPG signals for real-time health monitoring devices," *IEEE Access*, vol. 10, pp. 15707–15745, Jan. 2022.

[57] G. N. K. Reddy, M. S. Manikandan, and N. V. L. N. Murty, "Information theoretic metrics for automatic quality assessment of processed PPG signals," in *Proc. 3rd Int. Conf. Electr. Electron. Eng. (ICEEE)*, Bangladesh, Dec. 2021, pp. 157–160.

[58] F. Sartor, J. Gelissen, R. van Dinther, D. Roovers, G. B. Papini, and G. Coppola, "Wrist-worn optical and chest strap heart rate comparison in a heterogeneous sample of healthy individuals and in coronary artery disease patients," *BMC Sports Sci., Med. Rehabil.*, vol. 10, no. 1, p. 2018, Dec. 2018.

[59] *ANSI/AAMI Cardiac Monitors, Heart Rate Meters, and Alarms*, Amer. Nat. Standards Inst., Arlington, TX, USA, 2002.

[60] N. Saquib, M. T. I. Papon, I. Ahmad, and A. Rahman, "Measurement of heart rate using photoplethysmography," in *Proc. Int. Conf. Netw. Syst. Secur. (NSysS)*, Jan. 2015, pp. 1–6.

[61] M. A. Motin, C. K. Karmakar, and M. Palaniswami, "Modified thresholding technique of MMSPCA for extracting respiratory activity from short length PPG signal," in *Proc. 39th Annu. Int. Conf. IEEE Eng. Med. Biol. Soc. (EMBC)*, Jul. 2017, pp. 1804–1807.

[62] K. H. Shelley, A. A. Awad, R. G. Stout, and D. G. Silverman, "The use of joint time frequency analysis to quantify the effect of ventilation on the pulse oximeter waveform," *J. Clin. Monitor. Comput.*, vol. 20, no. 2, pp. 81–87, Jun. 2006.

[63] L. Gohlke, F. Dreyer, M. P. Álvarez, and J. Anders, "An IoT based low-cost heart rate measurement system employing PPG sensors," in *Proc. IEEE SENSORS*, Oct. 2020, pp. 1–4.

[64] I. A. E. Zaeni, Aripriharta, M. Jiono, D. R. Anzani, and L. Hernandez, "Implementation of adaptive threshold for peak detection of photoplethysmography applied on microcontroller," in *Proc. Int. Conf. Electr., Electron. Inf. Eng. (ICEEIE)*, Oct. 2019, pp. 226–229.

[65] R. Jaafar and M. A. A. Rozali, "Estimation of breathing rate and heart rate from photoplethysmogram," in *Proc. 6th Int. Conf. Electr. Eng. Informat. (ICEEI)*, Nov. 2017, pp. 1–4.

[66] A. M. Johnson, R. Jegan, and X. A. Mary, "Performance measures on blood pressure and heart rate measurement from PPG signal for biomedical applications," in *Proc. Int. Conf. Innov. Electr., Electron., Instrum. Media Technol. (ICEEIMT)*, Feb. 2017, pp. 311–315.

[67] S. Bagha and L. Shaw, "A real time analysis of PPG signal for measurement of SpO_2 and pulse rate," *Int. J. Comput. Appl.*, vol. 36, no. 11, pp. 45–50, Dec. 2011.

[68] S. G. Fleming and L. Tarassenko, "A comparison of signal processing techniques for the extraction of breathing rate from the photoplethysmogram," *Int. J. Biol. Med. Sci.*, vol. 2, no. 4, pp. 232–236, 2007.

GANGIREDDY NARENDRA KUMAR REDDY (Member, IEEE) received the B.Tech. degree in electronics and communication engineering from the JNTUA College of Engineering, Anantapur, India, in 2014, and the Ph.D. degree from the School of Electrical Sciences, IIT Bhubaneswar, India, in 2022. He is currently an Assistant Professor with the Department of Electronics and Communication Engineering, IIIT Kottayam, Kerala, India. His current research interests include biomedical signal processing, wearable healthcare monitoring, VLSI signal processing, machine learning, and the Internet of Things.

M. SABARIMALAI MANIKANDAN (Senior Member, IEEE) received the B.E. degree in electronic and communication engineering from Bharathiar University, Coimbatore, India, the M.E. degree in microwave and optical engineering from Madurai Kamaraj University, Madurai, India, and the Ph.D. degree in cardiovascular signal processing from the Department of Electronics and Communication Engineering, IIT Guwahati, Guwahati, India. He was an Assistant Professor with Amrita Vishwa Vidyapeetham University, Ettimadai, India. He was a Chief Engineer with the Advanced Technology Group, Samsung India Electronic Pvt. Ltd., Noida, India. He was an Assistant Professor with the Biomedical System Laboratory, School of Electrical Sciences, IIT Bhubaneswar, India. He is currently an Associate Professor of electrical engineering with the Indian Institute of Technology Palakkad. He has published more than 70 research papers in reputed journals and conference proceedings. His research interests include signal and image processing, adaptive machine learning, the Internet of Things, VLSI signal processing, machine learning architectures, application system development: health (human, machine, and structural) monitoring systems, audio and speech processing systems for human–machine interactions, biometric and data security for authentication and authorization, environmental monitoring systems for ambient assisted living, UAV-assisted IoT for smart surveillance systems, and context and quality-aware pattern learning networks for event recognition. He was a recipient of the 2012 Outstanding Performance Award during his tenure at Samsung India Electronic Pvt. Ltd. He served as a Reviewer for many reputed journals of the IEEE, IET, Springer, Hindawi, PLOS One, Frontiers, and Elsevier.

N. V. L. NARASIMHA MURTY (Member, IEEE) received the B.Tech. degree from Jawaharlal Nehru Technological University Hyderabad, Hyderabad, India, and the Ph.D. degree in electronics engineering from IIT Banaras Hindu University, now IIT(BHU), Varanasi, India. Since then, he has been working in various academic institutions in India. He is currently an Associate Professor with the Department of Electrical Engineering, Indian Institute of Technology Tirupati, Tirupati, Andhra Pradesh, India. His research interests include semiconductors for harsh environments and sensors and instrumentation. He is a Life Member of the Optical Society of India.

LINGA REDDY CENKERAMADDI (Senior Member, IEEE) received the master's degree in electrical engineering from the Indian Institute of Technology Delhi (IIT Delhi), New Delhi, India, in 2004, and the Ph.D. degree in electrical engineering from the Norwegian University of Science and Technology (NTNU), Trondheim, Norway, in 2011.

He was with Texas Instruments on mixed-signal circuit design before joining the Ph.D. Program with NTNU. After finishing his Ph.D. degree, he worked on radiation imaging for an atmosphere–space interaction monitor (ASIM mission to the International Space Station) with the University of Bergen, Bergen, Norway, from 2010 to 2012. He is currently a Leader of the Autonomous and Cyber-Physical Systems (ACPS) Research Group and a Professor with the University of Agder, Grimstad, Norway. He is a Principal Investigator and a Co-Principal Investigator of many research grants from the Norwegian Research Council. He is also quite active in medical imaging. His research interests include the Internet of Things (IoT), cyber-physical systems, autonomous systems, robotics and automation involving advanced sensor systems, computer vision, thermal imaging, LiDAR imaging, radar imaging, wireless sensor networks, smart electronic systems, advanced machine learning techniques, connected autonomous systems, including drones/unmanned aerial vehicles (UAVs), unmanned ground vehicles (UGVs), unmanned underwater systems (UUSs), 5G- (and beyond) enabled autonomous vehicles, and socio-technical systems like urban transportation systems, smart agriculture, and smart cities. He has coauthored more than 130 research publications that have been published in prestigious international journals and standard conferences in the above research areas.

Dr. Cenkeramaddi is a member of ACM. He is a member of the editorial boards of various international journals and technical program committees of several IEEE conferences. Several of his master's students received the Best Master's Thesis Award in Information and Communication Technology (ICT). He serves as a reviewer for several reputed international conferences and IEEE journals.